LBL-7051 c.2
SAC-19
UC-70

SWEDISH-AMERICAN COOPERATIVE PROGRAM ON RADIOACTIVE WASTE STORAGE IN MINED CAVERNS IN CRYSTALLINE ROCK

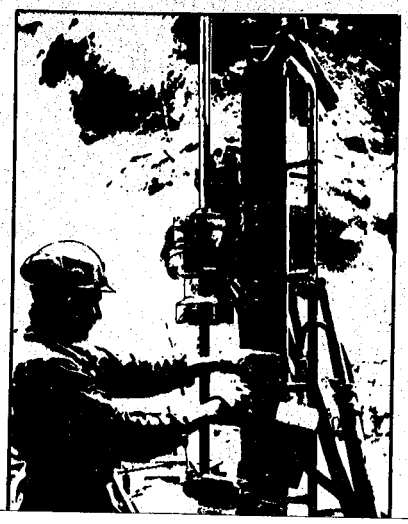

Technical Information Report No. 19

FRACTURE DETECTION IN CRYSTALLINE ROCK USING ULTRASONIC SHEAR WAVES

K. H. Waters and S. P. Palmer
Department of Materials Science and Mineral Engineering
University of California, Berkeley
and
W. E. Farrell
tems, Science, and Software
La Jolla, California

December 1978

TWO-WEEK LOAN COPY

This is a Library Circulating Copy which may be borrowed for two weeks. For a personal retention copy, call Tech. Info. Division, Ext. 6782

RECEIVED
LAWRENCE
BERKELEY LABORATORY

AUG 3 1979

LIBRARY AND
DOCUMENTS SECTION

A Joint Project of

Swedish Nuclear Fuel Supply Co.
Fack 10240 Stockholm, Sweden

Operated for the Swedish
Nuclear Power Utility Industry

Lawrence Berkeley Laboratory
Earth Sciences Division
University of California
Berkeley, California 94720, USA

Operated for the U.S. Department of
Energy under Contract W-7405-ENG-48

LBL-7051 c.2

FRACTURE DETECTION IN CRYSTALLINE ROCK USING ULTRASONIC SHEAR WAVES

K. H. Waters and S. P. Palmer
Department of Materials Science and Mineral Engineering
University of California, Berkeley

and

W. E. Farrell
Systems, Science, and Software
La Jolla, California

December 1978

This report was prepared by the Lawrence Berkeley Laboratory under the University of California contract W-7405-ENG-48 with the Department of Energy. Funding for this project is administered by the Office of Nuclear Waste Isolation at Battelle Memorial Institute.

PREFACE

This report is one of a series documenting the results of the Swedish-American cooperative research program in which the cooperating scientists explore the geological, geophysical, hydrological, geochemical, and structural effects anticipated from the use of a large crystalline rock mass as a geologic repository for nuclear waste. This program has been sponsored by the Swedish Nuclear Power Utilities through the Swedish Nuclear Fuel Supply Company (SKBF), and the U.S. Department of Energy (DOE) through the Lawrence Berkeley Laboratory (LBL).

The principal investigators are L. B. Nilsson and O. Degerman for SKBF, and N. G. W. Cook, P. A. Witherspoon, and J. E. Gale for LBL. Other participants will appear as authors of the individual reports.

Previous technical reports in this series are listed below.

1. Swedish-American Cooperative Program on Radioactive Waste Storage in Mined Caverns by P. A. Witherspoon and O. Degerman. (LBL-7049, SAC-01).

2. Large Scale Permeability Test of the Granite in the Stripa Mine and Thermal Conductivity Test by Lars Lundstrom and Haken Stille. (LBL-7052, SAC-02).

3. The Mechanical Properties of the Stripa Granite by Graham Swan. (LBL-7074, SAC-03).

4. Stress Measurements in the Stripa Granite by H. Carlsson. (LBL-7078, SAC-04).

5. Borehole Drilling and Related Activities at the Stripa Mine by Pavel J. Kurfurst, T. Hugo-Persson, and G. Rudolph. (LBL-7080, SAC-05).

6. A Pilot Heater Test in the Stripa Granite by Hans Carlsson. (LBL-7086, SAC-06).

7. An Analysis of Measured Values for the State of Stress in the Earth's Crust by Dennis B. Jamison and Neville G. W. Cook. (LBL-7071, SAC-07).

8. Mining Methods Used in the Underground Tunnels and Test Rooms at Stripa by B. Andersson and P. A. Halen. (LBL-7081, SAC-08).

9. Theoretical Temperature Fields for the Stripa Heater Project by Tin Chan, Neville G. W. Cook, and Chin-Fu Tsang. (LBL-7082, SAC-09).

10. Mechanical and Thermal Design Considerations for Radioactive Waste Repositories in Hard Rock. Part I: An Appraisal of Hard Rock for Potential Underground Repositories of Radioactive Wastes by Neville G. W. Cook; Part II: In Situ Heating Experiments in Hard Rock: Their Objectives and Design by Neville G. W. Cook and Paul A. Witherspoon. (LBL-7073, SAC-10).

11. Full-Scale and Time-Scale Heating Experiments at Stripa: Preliminary Results by Neville G.W. Cook and Michael Hood. (LBL-7072, SAC-11).

12. Geochemistry and Isotope Hydrology of Groundwaters in the Stripa Granite: Results and Preliminary Interpretation by P. Fritz, J.F. Barker, and J.E. Gale. (LBL-8285, SAC-12).

13. Electrical Heaters for Thermo-mechanical Tests at the Stripa Mine by R. H. Burleigh, E. P. Binnall, A. O. DuBois, D. U. Norgren, and A. R. Oritz. (LBL-7063, SAC-13).

14. Data Acquisition, Handling, and Display for the Heater Experiments at Stripa by Maurice B. McEvoy (LBL-7062, SAC-14).

15. An Approach to the Fracture Hydrology at Stripa: Preliminary Results by J. E. Gale and P. A. Witherspoon. (LBL-7079, SAC-15).

16. Preliminary Report on Geophysical and Mechanical Borehole Measurements at Stripa by P. Nelson, B. Paulsson, R. Rachiele, L. Andersson, T. Schrauf, W. Hustrulid, O. Duran, and K. A. Magnusson. (LBL-8280, SAC-16).

17. Observations of a Potential Size-Effect in Experimental Determination of the Hydraulic Properties of Fractures by P. A. Witherspoon, C. H. Amick, J. E. Gale, and K. Iwai (LBL-8571, SAC-17).

18. Rock Mass Characterization for Storage of Nuclear Waste in Granite by P. A. Witherspoon, P. Nelson, T. Doe, R. Thorpe, B. Paulsson, J. Gale, and C. Forster (LBL-8570, SAC-18).

Table of Contents

LIST OF FIGURES vi

LIST OF TABLES vii

ABSTRACT 1

1. INTRODUCTION 2

2. WAVE PROPAGATION IN AN ELASTIC MEDIUM 4

3. EXPERIMENTAL EQUIPMENT AND PROCEDURE 10

4. RESULTS OF S_H REFLECTION STUDY SIMULATING CRACK CLOSURE UNDER AN APPLIED STRESS 15

5. RESULTS OF S_H REFLECTION EXPERIMENTS CONCERNING THE DETECTION OF AN IRREGULAR, FLUID-FILLED CRACK 19

6. EXPERIMENTS ON METHODS OF REDUCING SURFACE WAVE NOISE 32

7. DECONVOLUTION PROCESSING 36

8. CONCLUSIONS AND RECOMMENDATIONS 42

9. ACKNOWLEDGMENTS 44

10. BIBLIOGRAPHY 46

LIST OF FIGURES

1. (A) Cartesian coordinate system used in separating shear and compressional components of the total displacement (B) Geometry used in derivation of the reflection coefficient for an interface between two different elastic media 5

2. Multiple reflections of an impulsive, plane P-wave normally incident on a water-filled crack 8

3. Experimental arrangement on laboratory granite slab. 10

4. A S_H source (S) and receiver (R) positioned on the largest face of a 1.0 μ x 0.65 μ x 0.30 μ granite slab 12

5. A multi-trace reflection record obtained by moving the receiver away from the source in equal increments. 13

6. Experimental arrangement used in measuring the reflection coefficient as a function of axial stress across a simulated crack. 16

7. Response of the S_H reflection coefficient as a function of axial stress across the lead-granite boundary. 17

8. Data showing the decrease in the amplitude of the reflected event as the axial stress across the lead block is increased . . . 18

9. Positions of S_H sources and profile lines on the circular face nearest the fracture of the cylindrical model 19

10. A multi-trace reflection record obtained along profile line L1L on Aug. 15, 1978 using a fixed S_H source and a movable S_H receiver. 21

11. A multi-trace profile recorded along line L1L on Aug. 25, 1978 . . 23

12. A multi-trace reflection profile recorded along line L2R on Aug. 15, 1978. 24

13. A multi-trace profile recorded along line L1L on Sept. 15, 1978. . 28

14. A profile recorded along line L1L on Sept. 20, 1978. 30

15. A profile recorded along line L1L on Sept. 20, 1978 with the crack and axial hole filled with water 31

16. A multi-trace profile recorded along L3I on Aug. 25, 1978 where the source and receiver are separated by a slit trench . . . 33

17. Profile recorded along L1R on Aug. 2, 1978 with a point S_H receiver. 35

18. A seismic trace recorded along line L1R on Aug. 3, 1978 using a 2" S_H linear receiver array 36

19. Waveform recorded directly beneath source on the far face of the rectangular granite slab. 38

20. Waveform recorded on the top surface of the granite slab with a source-receiver separation of 14cm. 39

21. Deconvolved version of the received signal s(t) shown in Fig. 20 40

LIST OF TABLES

1. Velocity data measured along survey lines shown in Fig. 9 25

2. Tabulation of the data used to calculate dip angle of the reflector 27

ABSTRACT

An ultrasonic shear wave reflection profiling system for use in the detection of water-filled cracks occurring within a crystalline rock mass is being tested in a laboratory environment. The first priority is to develop a source-receiver pair that will enable the detection of seismic energy reflected from the back face of a 1.0 m x 0.65 m x 0.30 m rectangular granite slab. We presently are able to produce very good results (i.e., the direct observation of the primary reflection and its first multiple) using a source-receiver pair that broadcast and receive horizontally polarized shear (S_H) waves. Because shear (S) waves should not propagate in a fluid (or into a fluid-filled crack), we concluded that S_H wave reflection techniques should theoretically yield the best results in the detection of water-filled cracks. However, natural cracks are not perfectly flat, so experiments testing these techniques were performed on an irregular tensile crack induced approximately 0.5 m below one circular face of a 1.0-m diameter, 1.8-m-long granite cylinder. We again obtained good reflection data from this irregular crack with the crack either air filled or water filled. During this last study, data were collected that suggest a frequency-dependent S_H wave reflection coefficient for a granite-water interface.

Waves that propagate along the free surface of a rock mass (surface waves) can severely hinder the detection of reflected events. We have investigated two methods of reducing this surface wave noise. The first technique uses physical obstructions (such as a slit trench) to scatter the surface waves. The second technique, commonly used in petroleum exploration seis-

mology, uses a linear array of receivers located on the free surface to cancel waves that are propagating parallel to the array (e.g., surface waves), thus enhancing waves with propagation vectors orthogonal to the linear array (e.g., reflected events). Deconvolution processing, which is simply the convolution of the inverse of the source input with the received output, was found to be another method useful in surface wave cancellation. We feel that the results of these experiments are very encouraging, and that further research should include a small-scale field test using shear wave reflection techniques.

1. INTRODUCTION

The future use of nuclear fission for electrical power generation will be feasible only if the radioactive by-products of the fission reaction can be suitably isolated from the environment. One solution to this problem, presently being studied by the Swedish-American Cooperative Program on Radioactive Waste Storage in Mined Caverns in Crystalline Rock, proposes to store the nuclear waste in an underground repository located in a very impermeable crystalline rock mass. The permeability within a crystalline rock formation is very dependent on the presence of interconnected fractures. Thus, identification of cracks and fissures near such an underground repository is important to insuring the success of this method of waste isolation.

The ultimate goal of our research is to perfect a high-frequency (5- to 100-kHz) seismic reflection profiling system that will enable detection of discontinuities that do not intersect the underground opening. If successful, this system would assist in the correlation of fracture patterns between test boreholes. This profiling system, with further refinement, could be used as

an inexpensive reconnaissance tool for crack detection where no borehole data are available. At present, however, this profiling system is reminiscent of the earliest pulse radar techniques, in that it employs a singly pulsed transducer to create the source waves. Receiving transducers are placed near the source to detect energy scattered from inhomogeneities near the source-receiver pair. Cracks, jointing and blasting fractures, gouge zones, and the like represent the type of inhomogeneities expected adjacent to a hard-rock underground repository.

This report details the development of a seismic profiling system that has been successful in using reflected shear (S) waves to detect artificial and natural cracks in large,laboratory rock specimens. Previous studies that have used compressional (P) wave reflection techniques to detect cracks in laboratory samples have been quite encouraging (Yu 1967, Yu and Telford 1973, Gupta 1972, Dampney et al. 1972). However, attempts at using P wave reflection techniques to detect in-situ fractures have met with only limited success (Gupta 1972, Price 1975). Evans (1959) conducted a successful series of laboratory scale shear wave reflection experiments, but his models were constructed of metal, rather than rock. We have not been able to locate any published study using ultrasonic S wave reflection techniques to locate in-situ discontinuities. Thus, in order to test the feasibility of such a survey, we decided to perform a number of model tests in the laboratory as a first step in our research. The results of our laboratory experiments are presented in this report.

2. WAVE PROPAGATION IN AN ELASTIC MEDIUM

Two kinds of elastic waves can propagate through an unbounded, homogeneous, isotropic, perfectly elastic medium. These are classified as:

a) Compressional (P) waves, which have a propagation velocity

$$\alpha = \sqrt{\frac{\lambda + 2\mu}{\rho}} ,$$

and

b) Shear (S) waves, which have a propagation velocity $\beta = \sqrt{\mu/\rho}$;

where μ = shear modulus of the medium

ρ = density of the medium

λ = Lamé constant .

In general $\mu = 0$ (thus $\beta = 0$) for fluids, so that shear waves cannot propagate in a fluid medium. The displacements associated with P waves are parallel to the direction of propagation, whereas the displacements of S waves are perpendicular to the propagation direction. Thus, in a Cartesian coordinate system it is possible to separate the total shear motion of a plane propagating elastic wave into its vertical and horizontal components, which are termed the S_V and S_H components of the shear wave motion (see Fig. 1A). When the boundaries of a multi-layered medium are parallel to the horizontal plane, the equation of motion of the S_H component becomes decoupled from the pair of equations that describe the P and S_V motions. This simplification in the mathematics that describes the S_H motion is very convenient, but is only applicable to certain planar geometries.

The assumption of perfect linear elasticity inherent in the previous development does not allow for the observed frictional dissipation of seismic energy. Thus, it is necessary to include a term that will account for this

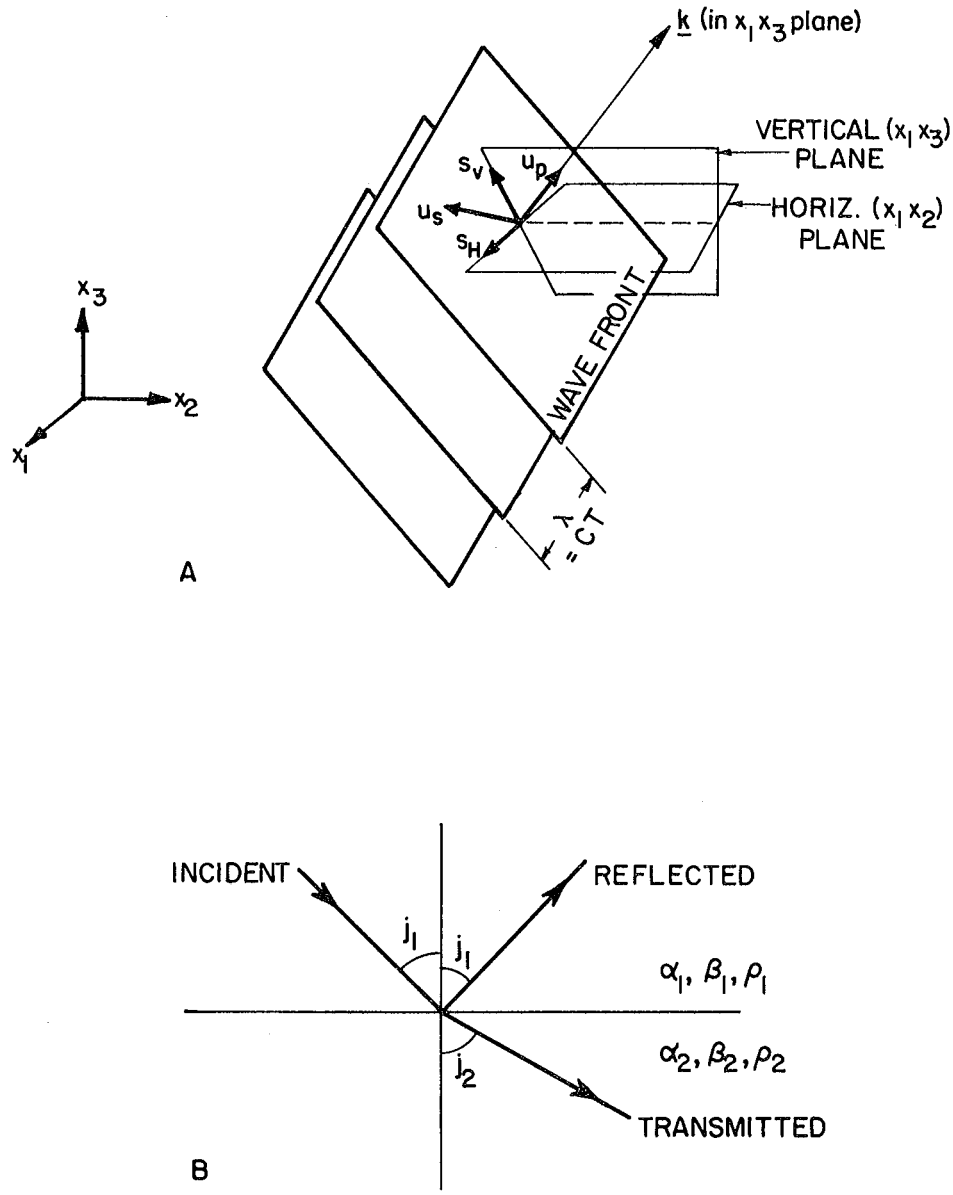

XBL 795-9774

Fig. 1. (A): Cartesian coordinate system used in separating shear and compressional components of the total displacement. U_p is the compressional component of displacement, and U_s is the shear component of displacement. $\underline{k}$ is the propagation vector of the plane wave. (B): Geometry used in derivation of the reflection coefficient for an interface between two different elastic media.

energy dissipation. If the attenuation is a result of solid frictional heating, then the amplitude of the dissipating wave will depend exponentially on the first power of frequency. For a plane wave with amplitude A_0 at position $\bar{r}_0$, the amplitude $A(\bar{r})$ of the wave at position $\bar{r}$ is given by:

$$A(\bar{r}) = \exp\left[-\frac{\pi f}{Qc}\,|\bar{r}-\bar{r}_0|\right] ,$$

where

f = frequency of the propagating wave

c = propagation velocity of the wave in the medium

$|r-\bar{r}_0|$ = distance between $\bar{r}$ and $\bar{r}_0$

Q = a "loss" constant which is a material property of the medium.

Finite size seismic sources, such as the S_H source used in this research, produce spherical waves rather than plane waves. The amplitude of a spherical wave decreases with increasing distance from the seismic source, as the total seismic energy of the spherical wave is spread out over the ever increasing surface area of the wavefront. This effect, termed geometrical spreading, has an r^{-1} spatial dependence for a point seismic source, where r is the distance from the point source to the observer.

When a propagating elastic wave encounters an interface between two different media (e.g., rock and water), part of the wave is reflected and part transmitted into the second medium. For the S_H component of a plane-propagating elastic wave incident on a horizontal planar boundary between two different media, it can be shown that the amplitude reflection coefficient (R_{SH}) is expressed by (see Fig. 1B):

$$R_{SH} = \frac{\sqrt{\mu_1\rho_1}\cos j_1 - \sqrt{\mu_2\rho_2}\cos j_2}{\sqrt{\mu_1\rho_1}\cos j_1 + \sqrt{\mu_2\rho_2}\cos j_2} .$$

For normal incidence, the amplitude reflection coefficient becomes:

$$R_{SH} = \frac{\sqrt{\mu_1\rho_1} - \sqrt{\mu_2\rho_2}}{\sqrt{\mu_1\rho_1} + \sqrt{\mu_2\rho_2}} = \frac{\rho_1\beta_1 - \rho_2\beta_2}{\rho_1\beta_1 + \rho_2\beta_2} .$$

Similarly, the amplitude reflection coefficient for a plane P wave normally incident on a planar boundary between two different media is:

$$R_p = \frac{\rho_1\alpha_1 - \rho_2\alpha_2}{\rho_1\alpha_1 + \rho_2\alpha_2} .$$

For a granite-water interface, $R_{SH} = 1.0$, and $R_p = 0.7688$, if we assume

for granite: $\alpha_1 = 4400$ m/s , $\beta_1 = 2700$ m/s , $\rho_1 = 2650$ kg/m^3,

for water: $\alpha_2 = 1524$ m/s , $\beta_2 = 0$, $\rho_2 = 1000$ kg/m^3.

Since $R_{SH} = 1.0$ (ignoring any small viscous coupling), then a horizontally polarized S wave is totally reflected from a granite-water interface. Thus, no S_H wave energy should penetrate a water-filled crack which has a nearly horizontal orientation. However, in a similar situation some P wave energy is transmitted into the water. The behavior of this transmitted energy depends strongly on the frequency of the P wave excitation, and on the thickness of the water-filled crack. Figure 2 shows that for a unit impulse input, the reflection consists of a series of pulses separated by the two-way travel time through the medium (water).

In order to show the effects of crack thickness (h) and frequency content of the incident P wave, we write the series of reflected pulses shown in

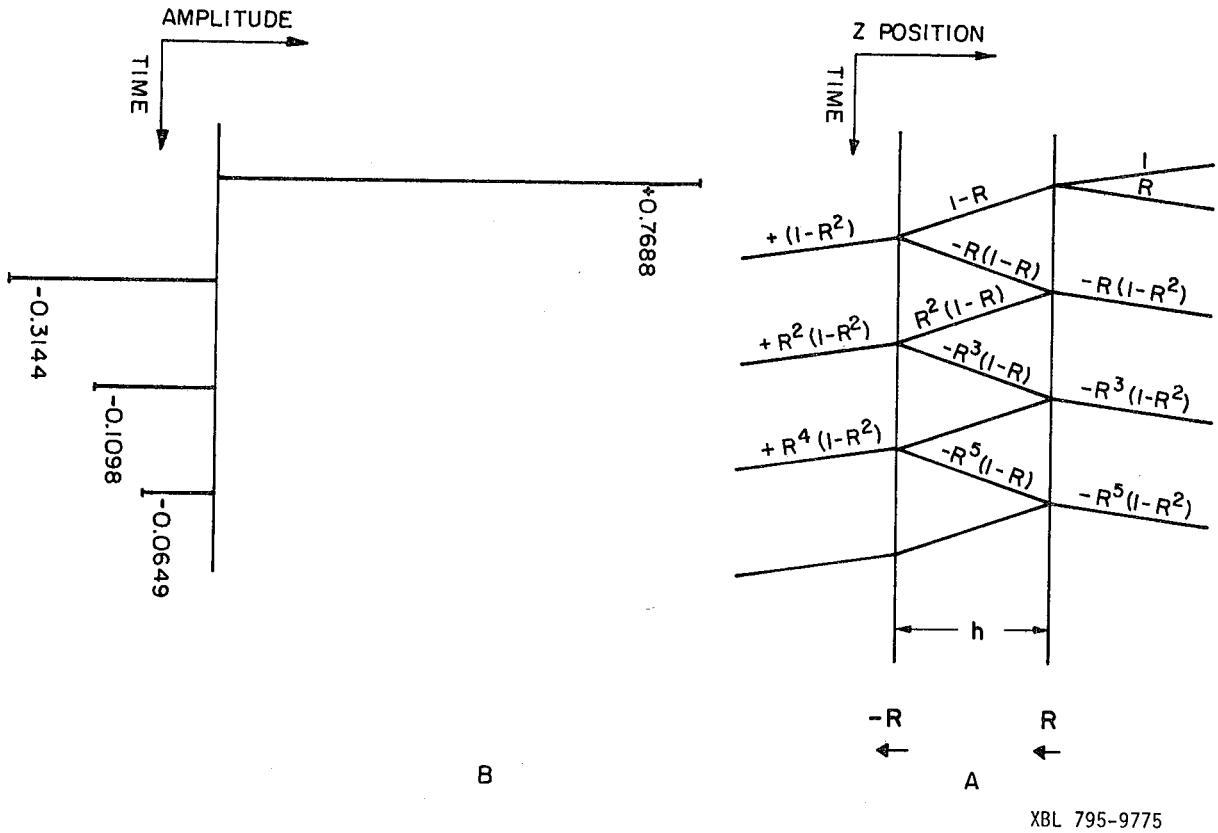

Fig. 2. Multiple reflections of an impulsive, plane P-wave normally incident on a water-filled crack. a) Wave-front loci and amplitudes plotted against the distance measured perpendicular to the plane of the crack (ordinate) and time (abscissa). b) The reflected pulse sequence when $R_p = 0.7688$, appropriate for $\rho_1\alpha_1 = 11.66 \times 10^6$ kg(s-m^2)$^{-1}$ (granite) $\rho_2\alpha_2 = 1.524 \times 10^6$ kg(s-m^2)$^{-1}$ (water). The time interval between pulses is the two-way travel time of a P-wave through the water layer.

Fig. 2 in the form:

$$a(t) = \sum_{n=0}^{\infty} a_n \, \delta(t - 2z/\alpha - 2n\Delta t)$$

where δ is the Dirac delta function, α is the P wave velocity in granite, z is the observer's distance above the upper crack boundary, and Δt is the one-way P wave travel time across the water-filled crack. The Fourier transform

of a(t), using the properties of the δ-function, the shift theorem, and the notation $E = \exp[-i2\pi f\Delta t]$ is:

$$A(f) = \left[e^{-i4\pi fz/\alpha}\right] \frac{R_p[1 - E^2]}{1 - R_p^2E^2}$$

For the squared modulus of A(f) we get:

$$|A(f)|^2 = 2R_p^2\left[\frac{1-\cos(4\pi f\Delta t)}{1+R_p^2-R_p^2\cos(4\pi f\Delta t)}\right]$$

from Born and Wolf (1975). Thus, as the product ($f\Delta t$) becomes small (the crack thickness becomes small compared to the wavelength of the P wave), then the modulus of the reflected pulses $|A(f)|$ goes to zero. This response severely limits the detection of thin, water-filled cracks using P wave reflection techniques. In theory, however, there should be no such frequency dependence for S_H waves incident on a fluid-filled crack.

Depending upon the given boundary conditions, various surface waves may propagate along the free boundary of a homogeneous or layered half-space. One type of surface wave, termed a Rayleigh wave, has a retrograde particle motion in the direction of propagation. The Rayleigh wave velocity is approximately 0.919β (for a Poisson's ratio $\sigma = 0.25$). Love waves are surface waves which have a particle motion lying along the free surface and at right angles to the propagation direction. Love waves are a result of the mutual interference of S_H waves trapped within the top surface layer. Surface waves are generally a source of undersirable noise in a seismic reflection experiment.

3. EXPERIMENTAL EQUIPMENT AND PROCEDURE

The equipment used in this experiment consists of:

piezoelectric ceramic plates polarized in the shear mode,

a high voltage pulse generator,

an oscilloscope for display of pulse and receiver signals,

a band-pass amplifier,

a boxcar integrator,

and an X-Y recorder (see Fig. 3).

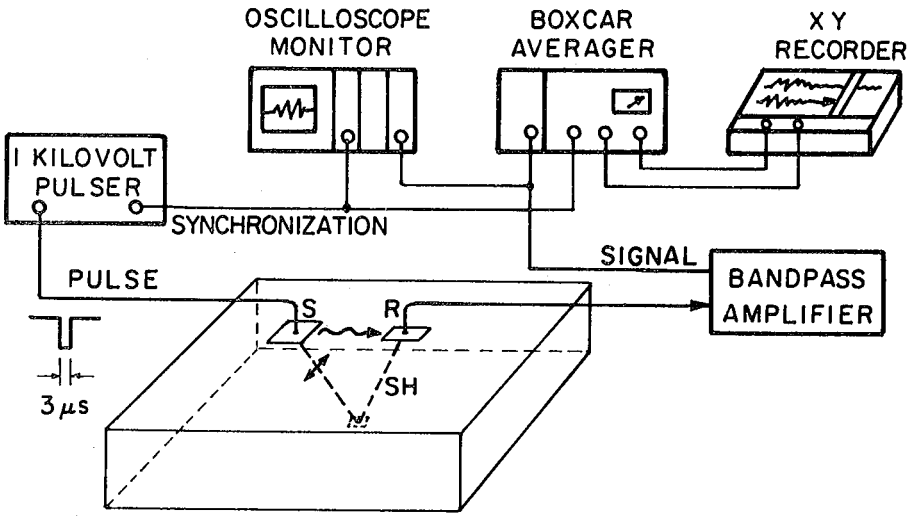

XBL 795-9776

Fig. 3. Experimental arrangement on laboratory granite slab. Source (S) emits elastic waves when an electric field is created across it. For suitably polarized material, and suitable plane of observation, the elastic wave is predominantly a horizontally polarized shear (SH) wave. Upon reflection from the lower granite surface, the wave travels up and impinges on receiver R, generating a proportional electrical voltage. Other waves pass directly from S to R, as shown by the wavy line and more complex reflected ray paths exist, some of which are sketched in Fig. 4.

A transient S_H elastic wave is launched into the rock slab by applying a large voltage pulse of ~3μs duration across the S_H source piezoelectric plate. This transient elastic wave results from the coupling of the strain and electric displacement fields within a piezoelectric material. The receiver is likewise a piezoelectric ceramic plate polarized so that S_H oriented particle motion will create a voltage across the two faces of the receiver plate. An excellent review of the piezoelectric phenomenon and its application in ultrasonics is presented in Mason (1964). This receiver signal is amplified and displayed on the oscilloscope. Also, a permanent, high-quality record is obtained by using the X-Y recorder in conjunction with the boxcar integrator. The boxcar integrator performs an analog averaging of a repetitive signal, thus increasing the signal/noise ratio. In addition, the averaging is performed slowly (at a controlled rate and over a controllable real-time span) so that the sweep rate of the oscilloscope is effectively reduced. The averaged signal can then be easily displayed on a standard X-Y recorder.

The two rock models used in this experiment are hewn from a very homogeneous, unweathered Sierran granodiorite. The first model used in the experiment is a 1.0 m x 0.65 m x 0.30 m rectangular slab with cut and polished faces. In order to simulate the irregular surface of a natural crack, a tensile fracture was induced approximately 0.5 m below one circular face of a 1.0-m-diameter, 1.8-m-long granodiorite cylinder, normal to the cylinder axis. The crack induced in this second model has approximately 8 cm of relief along its irregular surface, and appears very similar to jointing fractures found in natural settings.

The maximum separation of this crack along the circumference of the cylinder is observed to be 1/8 inch. A very thorough description of the cylindrical model (including photographs) is given in Witherspoon et al. (1977).

The first consideration in our model experiments was to obtain S_H reflections from the bottom surface of the rectangular slab. A S_H wave source (S) and receiver (R) were set up on the rectangular slab (see Fig. 4) so that S_H waves would propagate through the thin dimension of the model.

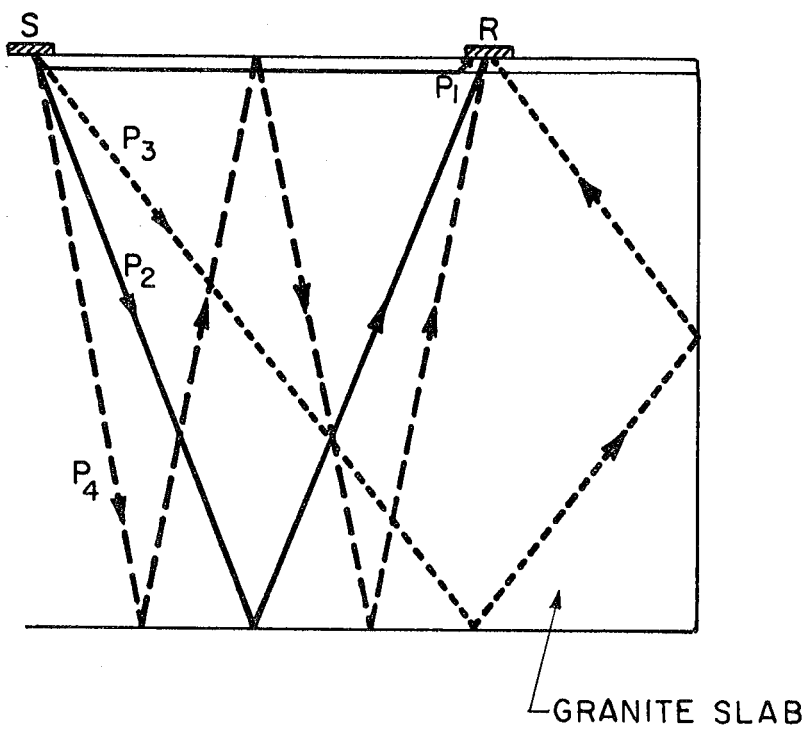

XBL 795-9777

Fig. 4. A S_H source (S) and receiver (R) are positioned on the largest face of a 1.0 m x 0.65 m x 0.30-m granite slab. Paths P_1, P_2, P_3, and P_4 represent various paths along which S_H waves can pass from source (S) to receiver (R). Path P_4 is termed the first multiple reflection.

The receiver was successively moved out in equal increments to more distant positions in order to obtain a multi-trace record, such as is shown in Fig. 5. Three separate events visible in these records are:

1) a direct S_H wave that travels along the surface from source to receiver (path P_1 in Fig. 4),

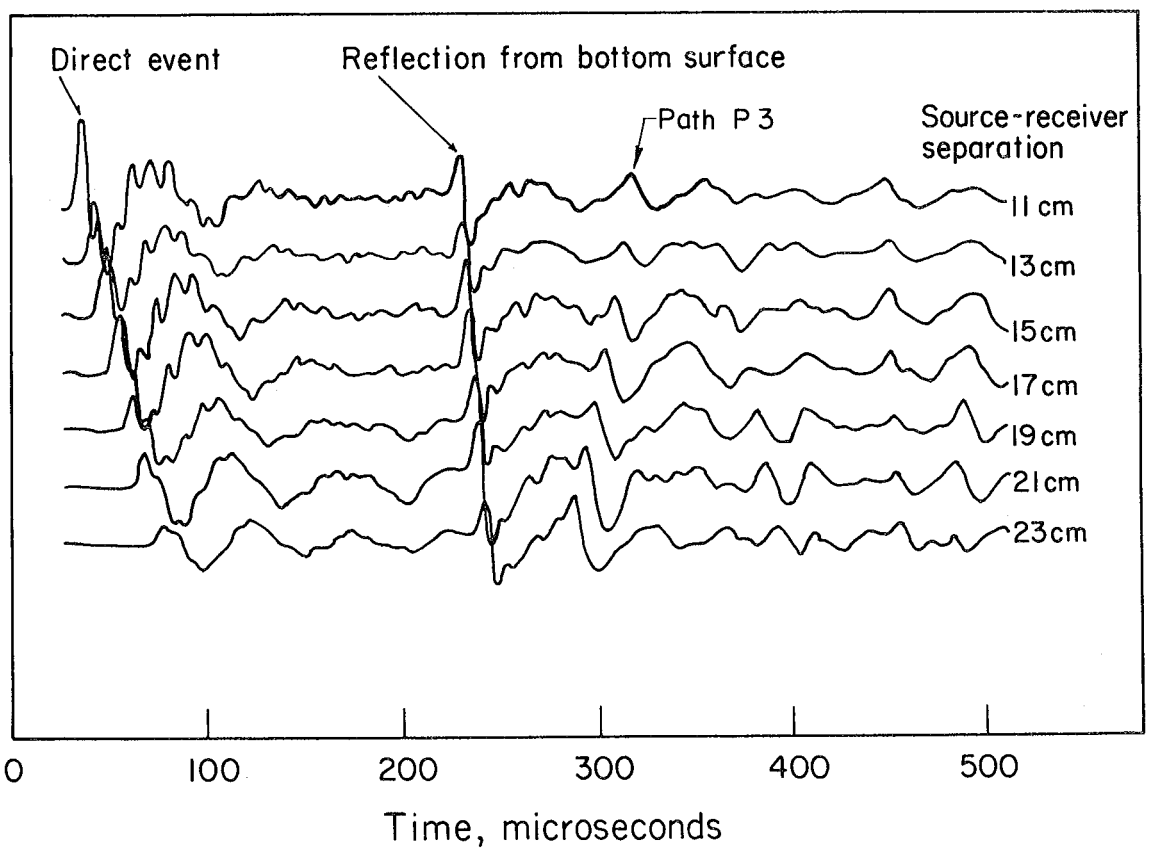

XBL 795-9771

Fig. 5. A multi-trace reflection record obtained by moving the receiver away from the source in equal increments. The direct event (path P_1 of Fig. 4) and the event reflected from the bottom of the granite slab (path P_2 of Fig. 4) are clearly visible. The event moving forward in time with increasing source-receiver separation is believed to correspond to path P_3 of Fig. 4. The slope of the direct event (P_1) corresponds to a shear wave velocity of β = 2.60 km/s, and the X^2-T^2 slope of the reflected event corresponds to a shear wave velocity of β = 2.65 km/s.

2) a S_H wave that is simply reflected from the bottom free surface of the slab (path P_2 in Fig. 4),

3) a reflected S_H wave that has a more complex path involving an additional reflection from the back vertical face of the model (path P_3 in Fig. 4).

The moveout of an event on such a multi-trace record (i.e., the deviation in arrival time as the source-receiver separation is increased) contains information regarding the ray-path geometry of the event. Events that travel directly along the surface from source to receiver (e.g., path P_1 of Fig. 4) have a linearly increasing moveout (direct event of Fig. 5). Events that have been reflected from a boundary or scatterer (e.g., path P_2 of Fig. 4) will have a hyperbolically increasing moveout (e.g., reflected event of Fig. 5).

Obtaining a good estimate of the propagation velocity of the media is critical in the interpretation of the S_H reflection data. Because the phase and propagation velocities are equal for an angle of incidence $j = 90°$ ($C = \beta/\sin j$), we may use the slope of the direct path (P_1) moveout as an estimate of the propagation velocity. The second estimate of the propagation velocity can be made from a standard X^2-T^2 plot of the reflection event arrival times, assuming that the reflector has a horizontal dip angle. Thus, we have two independent methods of measuring the S wave velocity of our rectangular model. Since the raypaths of the direct and reflected events sample different spatial regions within the slab, comparison of these two velocity estimates will give some indication regarding the degree of velocity inhomogeneity within the model. It should be noted that the apparent velocity obtained from the X^2-T^2 plot depends very strongly on the dip of the

reflector, and this apparent velocity is only identical to the propagation velocity of the media when the reflector is flat-lying. From the data presented in Fig. 5, one obtains a shear wave velocity β = 2.60 km/s from the direct S_H event, and a velocity β = 2.65 km/s from an X^2-T^2 plot of the reflection event. These values lie within the ranges of experimental error, and indicate that the shear wave velocity of the granite slab is reasonably homogeneous.

4. RESULTS OF S_H REFLECTION EXPERIMENT SIMULATING CRACK CLOSURE UNDER AN APPLIED STRESS

Repeated experiments on the rectangular slab clearly demonstrated our ability to receive S_H energy reflected from the bottom surface of the slab model. We then designed an experiment to study the effect of a simulated crack closure on the amplitude of a S_H pulse reflected from the crack. A crack was simulated by pressing a lead block to the rock slab at the reflection point of a source-receiver pair. The experimental arrangement is shown in Fig. 6. The supposition of this experiment is that some of the energy contained in the reflected event will "leak" into the lead block upon incidence, consequently reducing the received amplitude of this event. The reduced amplitude may be interpreted as resulting from a change in the reflection coefficient of the "crack": As the axial stress across the lead block is increased, the reflection coefficient of the "crack" varies. Figure 7 shows the typical response of the reflection coefficient and the axial stress across the "crack." The data presented in Fig. 8 clearly show the decrease in the reflected pulse amplitude as the axial load on the lead

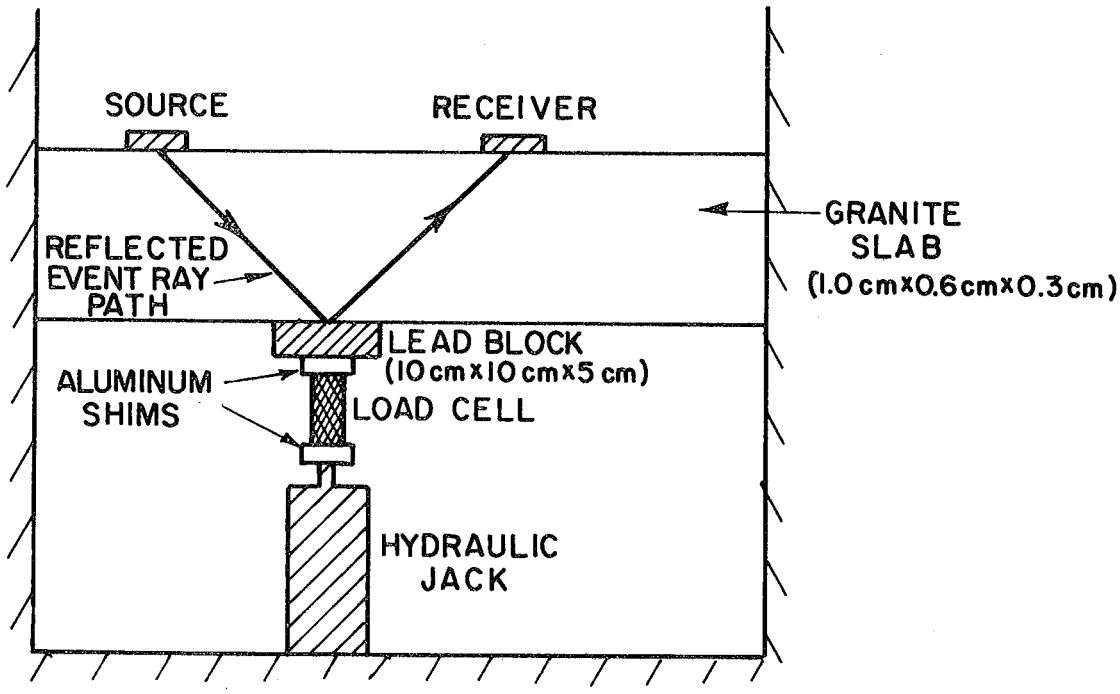

XBL 795-9778

Fig. 6. Experimental arrangement used in measuring the reflection coefficient as a function of axial stress across a simulated crack. Note the importance of locating the lead block at the reflecting point of the source-receiver pair. The characteristic shear wave impedance (product of density ρ and shear wave velocity β) is:

for lead,

$$Z_L = \rho_L \beta_L = (11.34\text{x}10^3 \text{ kg/m}^3)\ (700 \text{ m/s}) = 7.94\text{x}10^6 \text{ kg } (\text{-m}^2)^{-1}$$

for granite, $Z_g = \rho_g \beta_g = (2650 \text{ kg/m}^3)(2700 \text{ m/s}) = 7.16\text{x}10^6 \text{ kg } (\text{s-m}^2)^{-1}$.

Thus, the reflection coefficient R_{SH} for the granite-lead interface is $R_{SH} = +0.05$ for a normally incident plane wave.

block is increased. Because the shear wave impedances (product of the density and shear wave velocity) of lead and granite are nearly equal, we believe this experiment will give the approximate behavior of an air-filled rock fracture being closed by a uniaxial load.

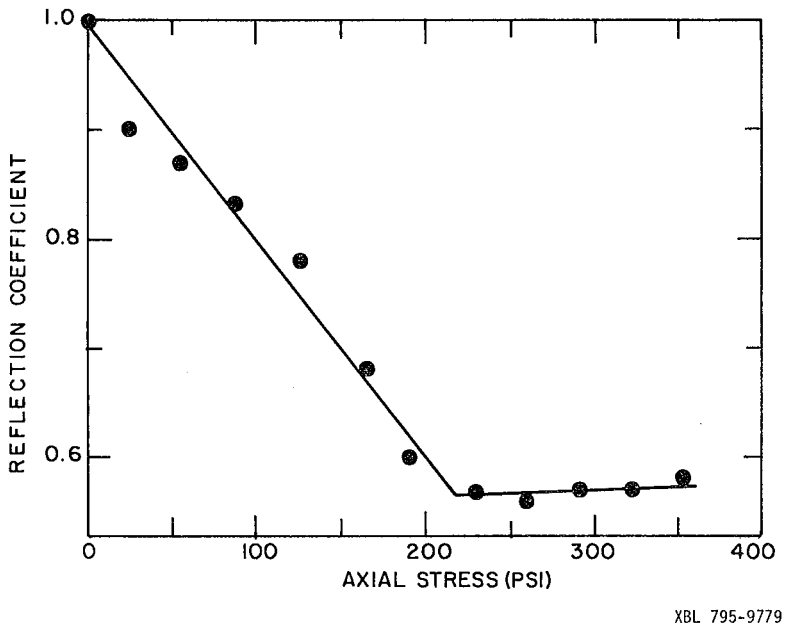

Fig. 7. Response of the S_H reflection coefficient as a function of axial stress across the lead-granite boundary. It is assumed that total reflection (R_{SH} = 1.0) occurs when the lead block is removed from the reflecting point (i.e., there is no axial stress). Figure 8 shows some of the reflection data used to determine the reflection coefficient response presented in this figure.

Repeated experiments have demonstrated that the response shown in Fig. 7 is representative. The reflection coefficient decreases linearly as the load is applied, until a stress of approximately 225 psi is reached. The reflection coefficient then remains relatively constant as the stress is further increased. The reflection coefficient appears to be directly dependent on the amount of contact area between the lead block and granite surface. The initial linear decrease of the reflection coefficient as the axial stress is applied probably results from the effective increase in contact area as the lead block is deformed to fit into the micro-irregularities of the granite surface. When most of these irregularities have been filled, further

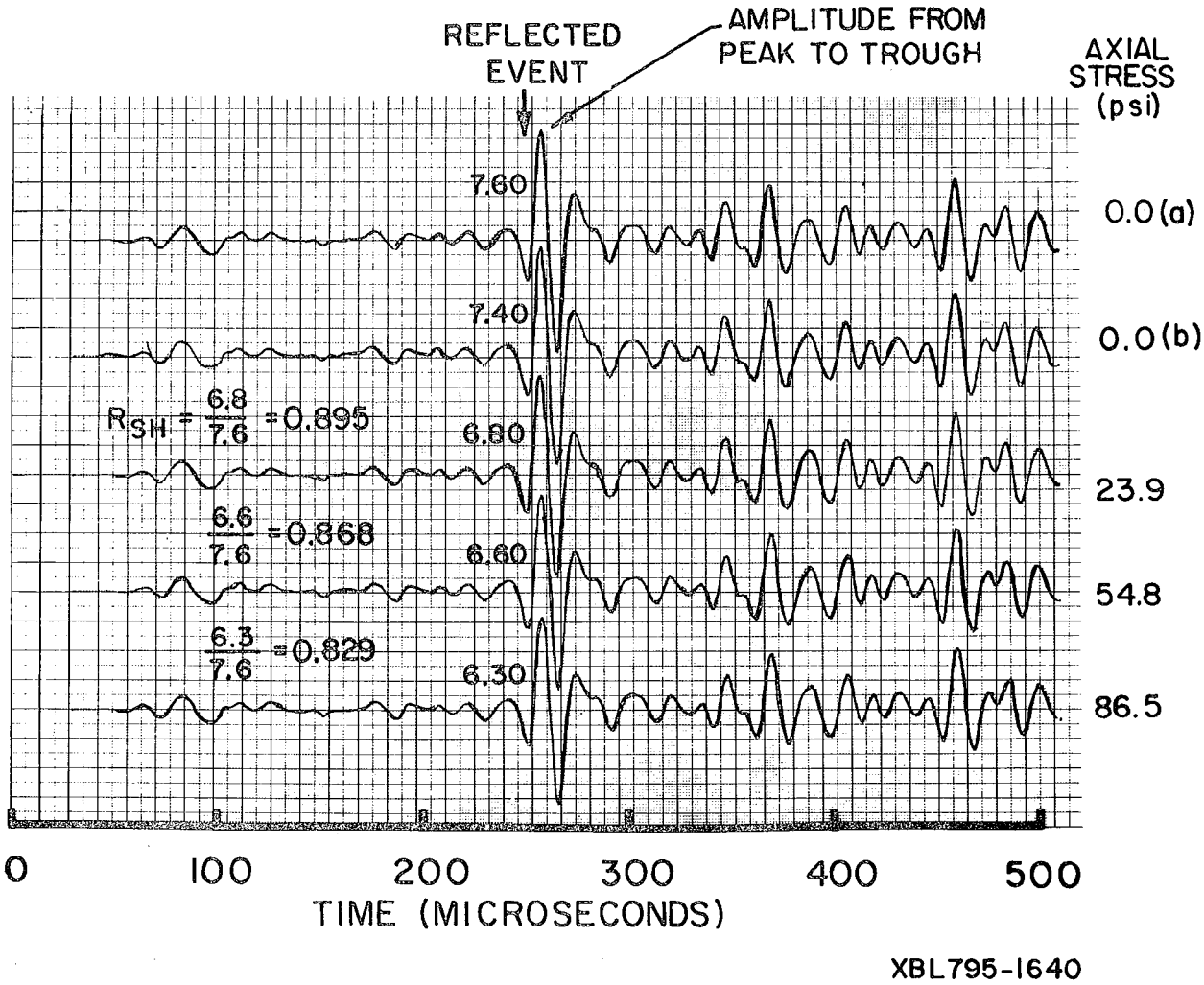

Fig. 8. Data showing the decrease in the amplitude of the reflected event as the axial stress across the lead block is increased. The reflection coefficient is obtained by dividing the amplitude (measured from peak to following trough) of the reflected event at a given axial stress by the reflected event amplitude when the lead block is not in contact with the granite slab. These data were used to obtain the first four data points shown on the graph of Fig. 7.

loading will not produce any change in the contact area, and consequently the reflection coefficient will remain unchanged. The significant result of this experiment is that it is possible to alter the reflection coefficient

across the reflecting boundary by varying the normal stress across this interface.

5. RESULTS OF S_H REFLECTION EXPERIMENTS CONCERNING THE DETECTION OF AN IRREGULAR, FLUID-FILLED CRACK

Naturally occurring fractures are not perfectly flat, but are rather rough and irregular. Thus, we thought it necessary to verify that our S_H

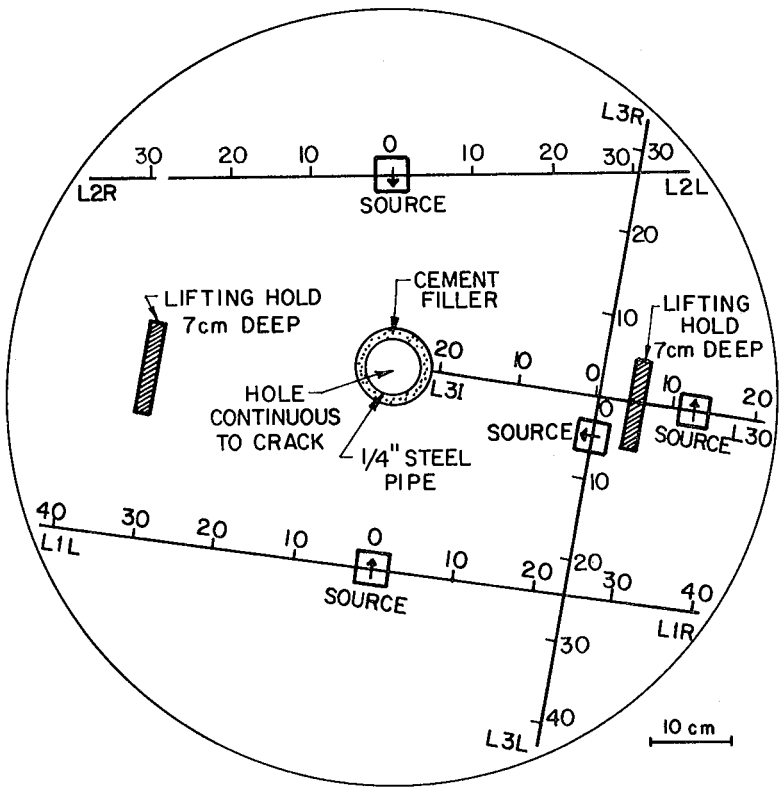

XBL 795-9780

Fig. 9. Positions of S_H sources and profile lines on the circular face nearest the fracture of the cylindrical model. The hole located in the center of the circular face continues axially downward until it reaches the fracture surface. This tensile fracture is approximately 0.5 m below the circular face shown in this figure, and is normal to the cylinder axis. The two 7-cm-deep lifting holds were used for transporting the cylinder at the quarry.

reflection profiling technique would successfully detect fractures with irregular surfaces. For this purpose a large, fractured, granite cylinder (described in Section 2) was acquired, and numerous profile lines (shown in Fig. 9) were surveyed along the circular face of the cylinder nearest the crack. A hole drilled axially from the circular face to the fracture prevented the location of profile lines near the center of the circular face (see Fig. 9). When the upper and lower sections of the fractured cylinder are fit back together, a crack is created that is relatively thin with respect to the wavelengths contained in the incident S_H pulse (wavelengths of 2.5 cm to 25 cm for frequencies of 100 kHz and 10 kHz, respectively). This crack was air-filled in all cases except during a series of experiments in which the response of a water-filled crack was studied.

The S_H sources were bonded to the rock surface with a fast-setting epoxy at the positions shown in Fig. 9. A movable S_H receiver, loaned to us by Prof. L. R. Johnson, was used in obtaining multi-trace records similar to the record shown in Fig. 5. In order to utilize the full operating range of the boxcar integrator, the amplifier gain was continually increased to compensate for increased source-receiver separations so that the amplitude of the direct event remained relatively constant.

Figure 10 shows the multi-trace record obtained along profile line L1L on August 15, 1978. Numerous seismic events are visible on this record, but only three of these events are easily identified. Event A in Fig. 10 represents the first detectable seismic energy in the record. This event probably represents some sort of "parasitic" P wave energy created by the S_H source, that travels along the most direct path from source to receiver (i.e.,

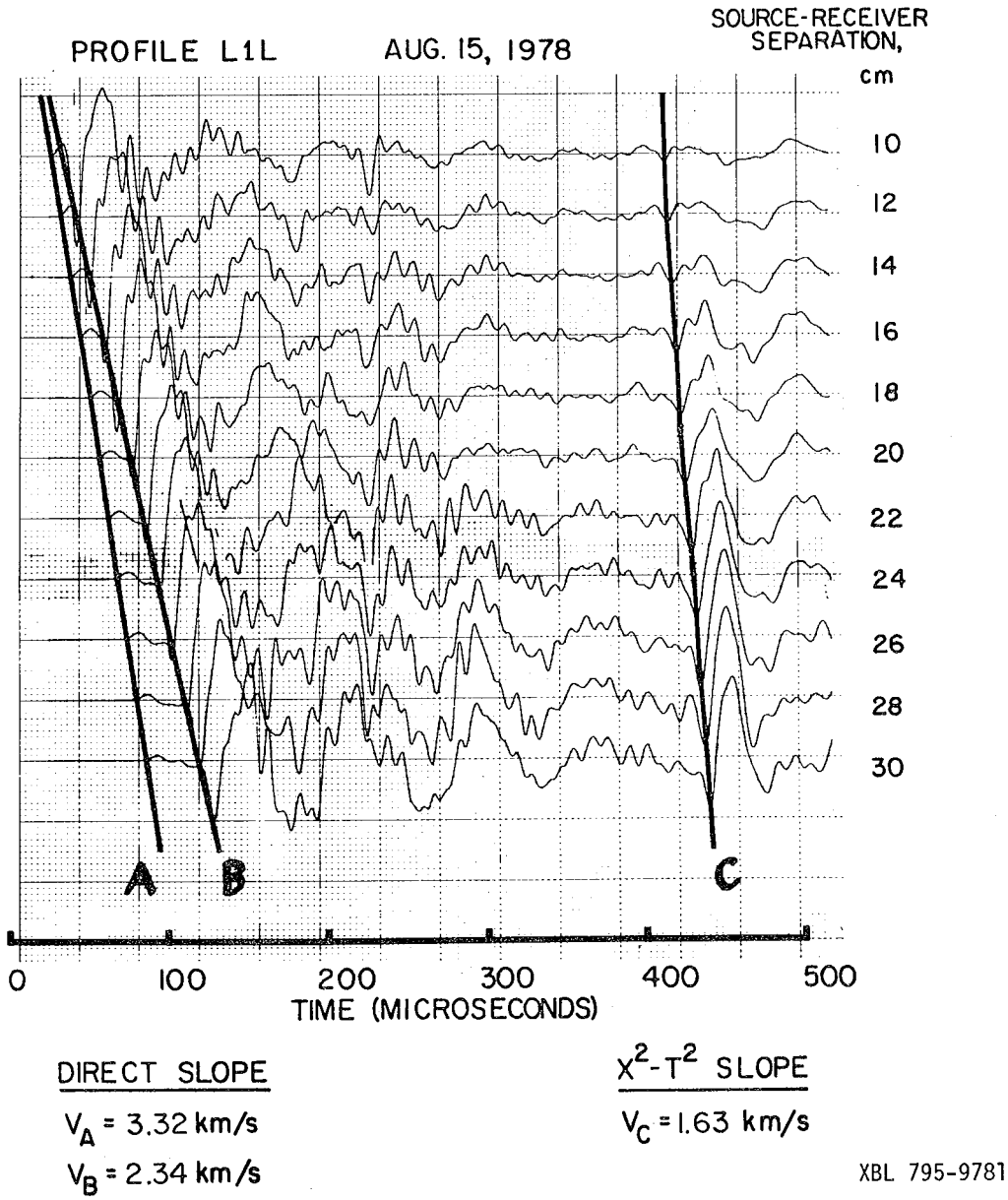

Fig. 10. A multi-trace reflection record obtained along profile line L1L on Aug. 15, 1978 using a fixed S_H source and a movable S_H receiver. Event A is a direct P wave, event B is a direct S_H wave, and event C is a S_H wave reflected from the air-filled tensile fracture. The large amplitude events occuring between 120 μs and 300 μs probably are reflections and diffractions from the axial hole located at the center of the circular face. The slopes of straight lines A and B are used to obtain the P and S wave velocities ($V_A = \alpha$ and $V_B = \beta$). For a horizontal reflector the X^2-T^2 velocity (V_C) should be the same as the direct velocity V_B, assuming that the model has a homogeneous shear wave velocity. Thus, either the crack is dipping beneath L1L, or the velocity beneath L1L is very (unreasonably) low.

along or just under the free surface). The large amplitude pulse, designated event B, is most likely an S_H wave traveling along a similar direct path from source to receiver. Because of its arrival time and hyperbolic moveout, event C of Fig. 10 is thought to be the S_H reflection from the air-filled crack. The numerous, large amplitude events that are visible in the portion of the record between 100 μs and 300 μs are believed to result from seismic energy diffracted by the axial hole located at the center of the circular face. Ray-path tracing indicates that such diffraction events should indeed arrive along this portion of the record.

Figure 11 presents a check on the repeatability of the data obtained during our seismic profiling experiments. This figure presents the multi-trace record obtained along profile line L1L on August 25, 1978, and so should be compared to Fig. 10. The comparison between these two records is good, and indicates that the errors inherent in repositioning the receiver are not overwhelming. Figure 12, a multi-trace record obtained along profile line L2R, shows that it is possible to detect the S_H crack reflection event along profile lines other than L1L.

Table 1 lists the measured data and mean P and S wave velocities along each profile line obtained from the direct P and S events. The S wave velocity appears to be fairly constant along this face of the cylinder, but the P wave velocity seems to vary spatially along this face. It appears that the direct P wave velocity increases as one moves from L2R toward L1R. Also, the measured P wave velocities (ranging from 3.16 to 3.69 km/sec) are much slower than the typical in-situ P wave velocities reported for granites, which range from 4.0 to 5.7 km/sec (Dobrin 1960). We believe that the slow

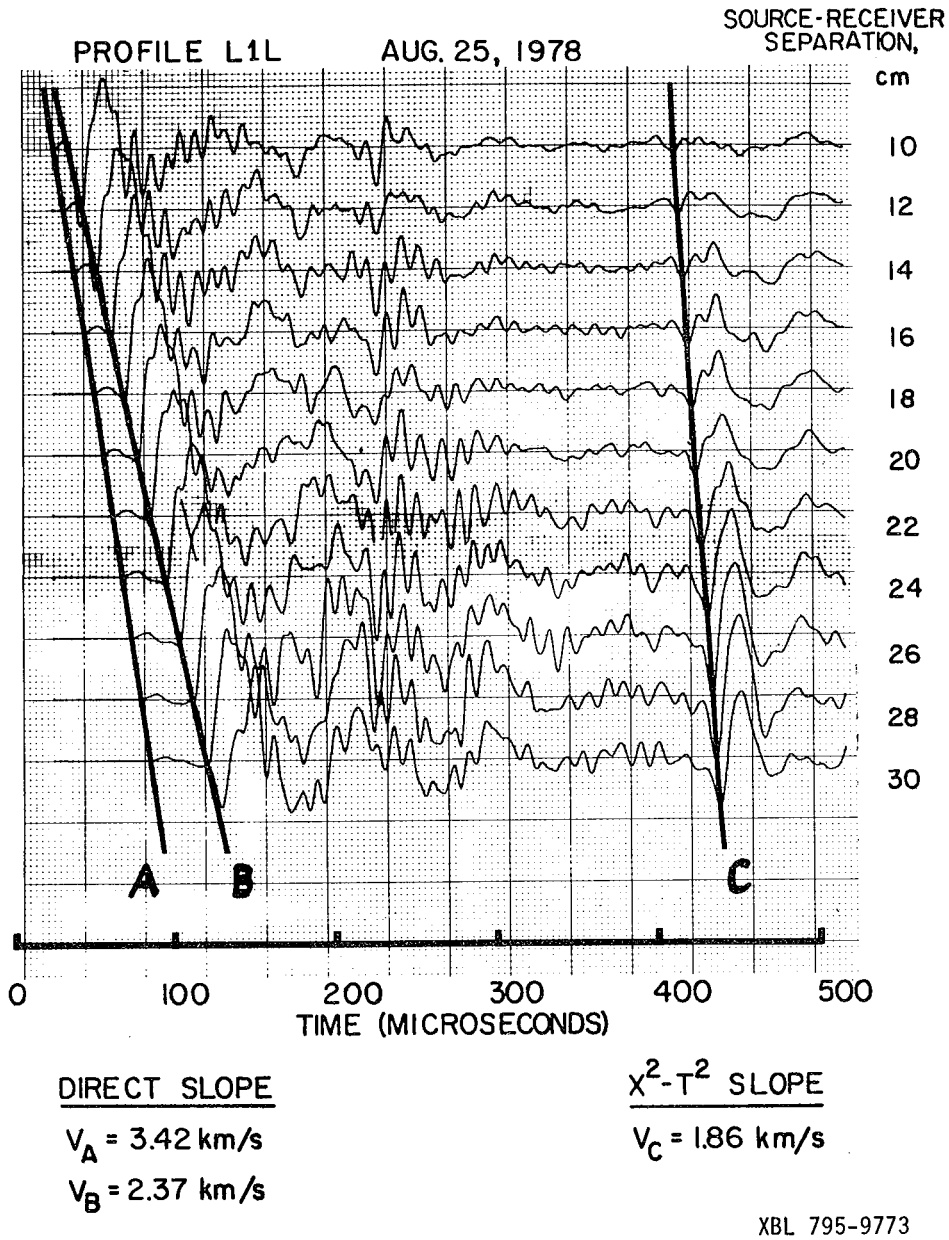

Fig. 11. A multi-trace profile recorded along line L1L on Aug. 25, 1978. Comparison of this figure to Fig. 10 will give an estimate of the repeatability of the experimental technique.

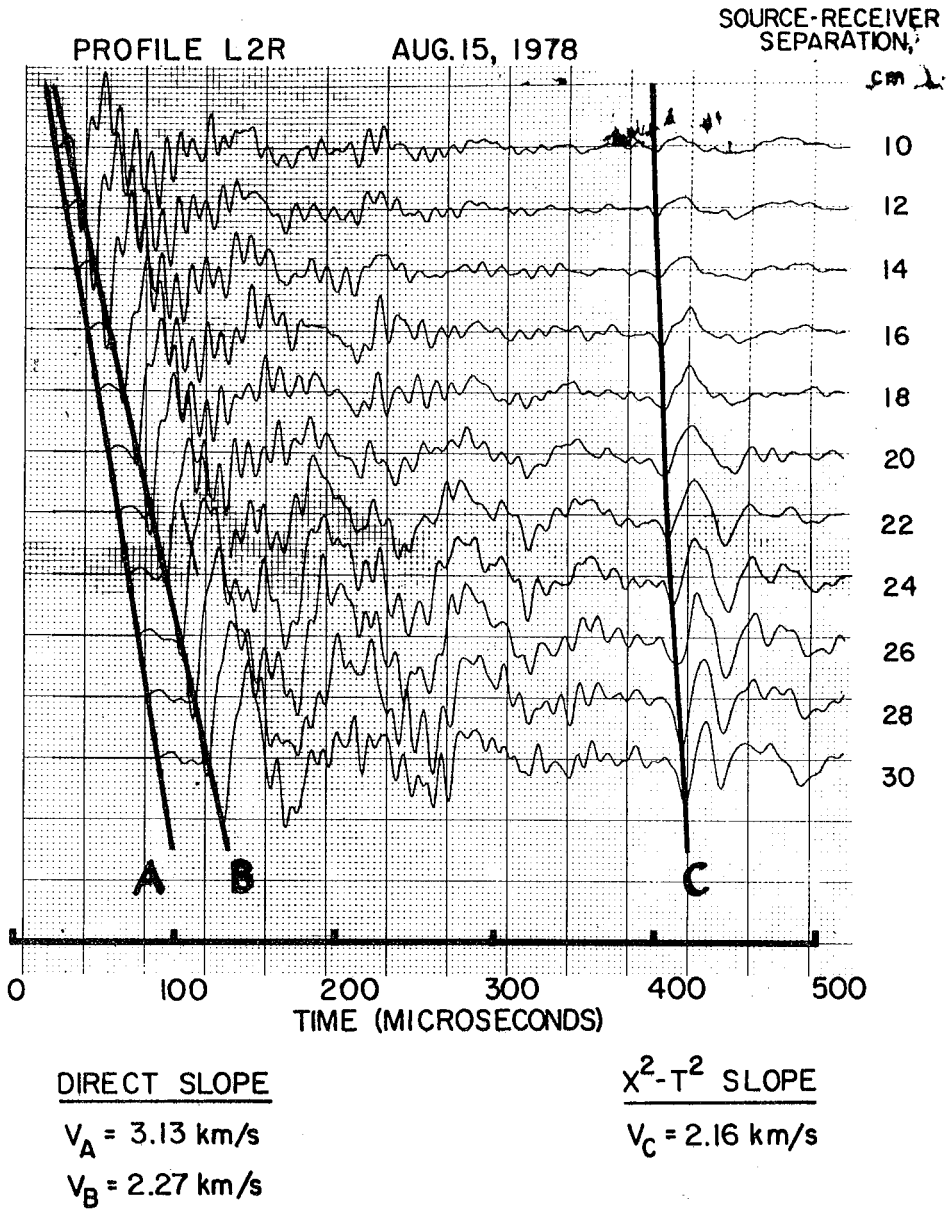

Fig. 12. A multi-trace reflection profile recorded along line L2R on Aug. 15, 1978. Note the similarity with profiles recorded along L1L, including the reflection event C.

Table 1. Velocity data measured along survey lines shown in Fig. 9.

Profile line	Measured values of α (km/s)	Mean α (km/s)	Standard deviation of mean α (km/s)	Measured values of β (km/s)	Mean β (km/s)	Standard deviation of mean β (km/s)
	3.42			2.38		
L1L	3.32	3.39	±0.08	2.34	2.36	±0.04
	3.42			2.37		
	3.40			2.34		
	3.52			2.54		
L1R	3.58	3.59	±0.08	2.45	2.47	±0.08
	3.63			2.43		
	3.61			--		
	3.24			2.28		
L2L	3.33	3.32	±0.14	2.38	2.37	±0.21
	3.29			2.29		
	3.43			2.54		
	3.25			2.36		
L2R	3.13	3.16	±0.11	2.27	2.30	±0.07
	3.17			2.30		
	3.10			2.28		
	3.72			2.34		
L3L	3.69	3.69	±0.09	2.52	2.41	±0.14
	3.62			2.37		
	3.74			2.42		
	3.34			2.36		
L3R	3.40	3.34	±0.08	2.26	2.31	±0.07
	3.32			--		
	3.29			--		

Note: The compressional (α) and shear (β) wave velocities are obtained from the slopes of the direct events.

P wave velocity measured along the face of the cylindrical model is probably due to the numerous axial load tests performed on this specimen during previous unrelated experiments.

For a dipping reflector, the apparent velocity derived from a X^2-T^2 plot of the reflection arrival times will not equal the propagation velocity. The X^2-T^2 velocity for L1L shows that the crack (reflector) has a significant amount of dip beneath this profile line. By combining the reflection data from L1L (Fig. 10) and L1R (Fig. 17, page 35) to obtain a symmetrical spread, we can use a derivation given by Telford et al. (1976) to obtain the dip angle of the reflector (angle from the horizontal). In this analysis only data from source-receiver separations of 20 cm or less are used, so that the assumption of constant reflector dip will be valid. Table 2 tabulates the data used in the calculation, and the resulting computed dip angle. These computed dip angles are very comparable to the observed dip of the fracture surface beneath the source common to profile lines L1L and L1R, which varies from 3° to 6° beneath line L1.

Figure 13 shows the multi-trace record obtained along profile line L1L on September 15, 1978, which is about two months after the S_H source plate was epoxied in position on the rock specimen. Comparing this record to pre-previous surveys along L1L, one observes a considerable increase in the high frequency (80- to 100-kHz) content of this record. We believe that the increased "ringing" of this later record is due to the deterioration of the epoxy bond between the piezoelectric source plate and the rock surface. With a good epoxy bond, most of the seismic energy created by the applied voltage pulse is immediately transmitted into the rock medium. Some seismic energy is not transmitted into the rock, and so remains "trapped" within the source plate. This "trapped" energy is internally reflected within the source plate, and consequently causes the source to "ring" at a

Table 2. Tabulation of data used to calculate dip angle of the reflector.

d (cm)	t_1 along L1L (μs)	t_2 along L1R (μs)	α L1L down-dip from source (degrees)
10	413.0	406.2	4.7
12	414.5	407.0	4.3
14	417.5	408.1	4.6
16	420.5	407.7	5.5
18	422.0	410.0	4.6
20	425.4	413.4	4.1

Note: From Telford et al. (1976), the dip angle Θ of a reflector is given by:

$$\Theta = \sin^{-1}\left[\frac{\beta(t_1-t_2)}{2d}\right] ,$$

where d = source - receiver separation

t_1 = arrival time of reflection event on down-dip receiver

t_2 = arrival time of reflection event on up-dip receiver

β = shear wave velocity .

Data used in this analysis are taken from line L1L (Fig. 10) and line L1R (Fig. 17). The shear wave velocity β is the average of the mean velocities along L1L and L1R given in Table 1, i.e., β = 2410 M/S.

Average Dip is 4.6° with L1L down-dip from the source.

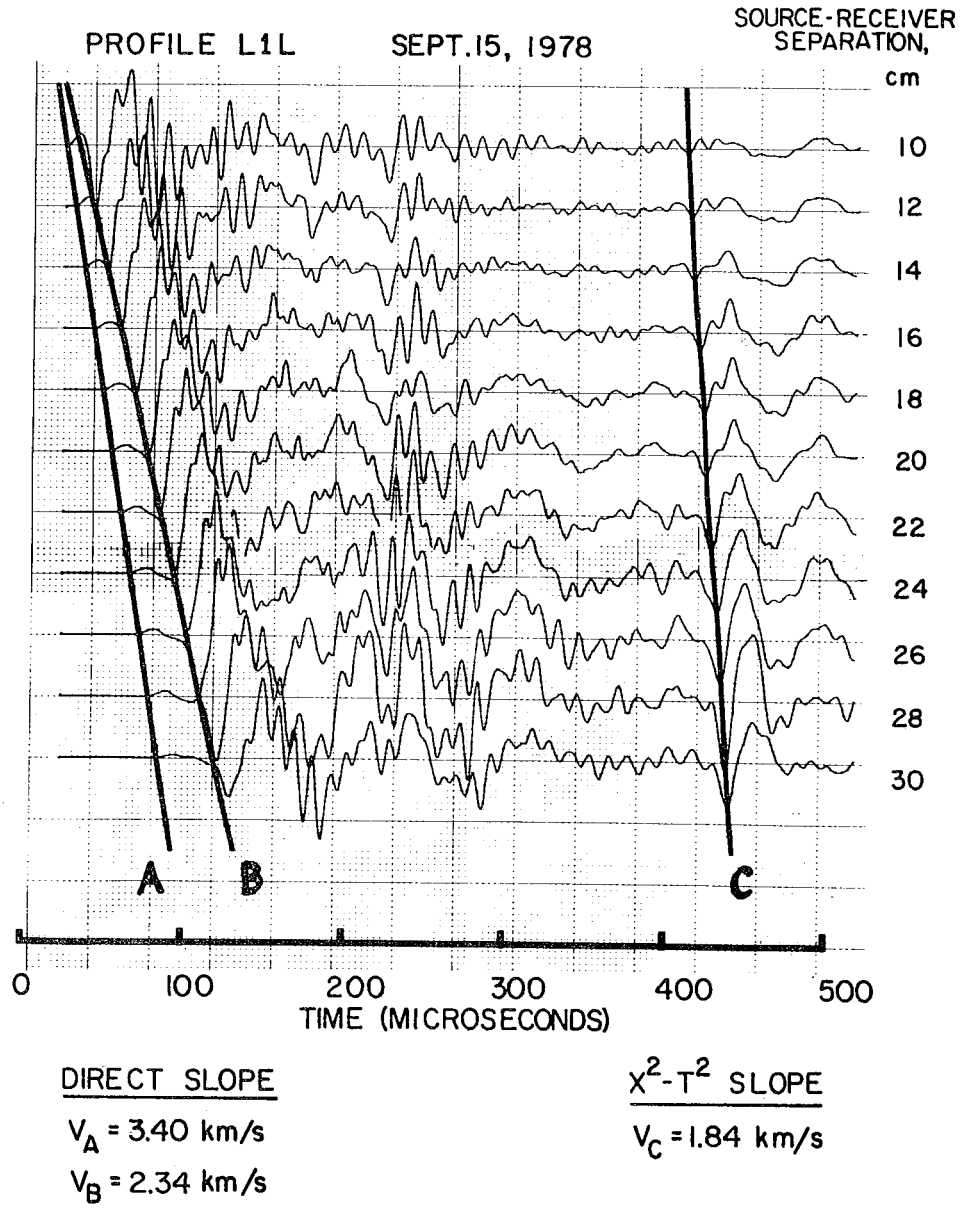

XBL 795-9790

Fig. 13. A multi-trace profile recorded along line L1L on Sept. 15, 1978. Note the "ringiness" of this record when compared to previous profiles along L1L (Fig. 10).

resonant frequency determined by the thickness of the plate (the fundamental S_H thickness mode). The piezoelectric source plates used in our experiment have an S_H thickness mode resonant frequency of approximately 100 kHz. As the epoxy bond deteriorates, less energy contained in the initial pulse will be transmitted into the rock medium, and consequently more energy remains "trapped" within the source plate. Thus, as the epoxy bond deteriorates, the source plate "rings" with a larger amplitude at its resonant frequency. We believe that a deteriorating epoxy bond is the primary cause of the large-amplitude (90- to 100-kHz) energy visible on the record shown in Fig. 13, and on all profiles subsequently recorded along L1L.

Figure 14 shows a multi-trace record obtained along L1L on September 30, 1978 (in this case the crack is air-filled). Note the significant amount of high frequency energy visible in this record, presumably due to the effect of source bonding. Figure 15 presents another record obtained along L1L on September 20, 1978; in this case the crack and axial hole have been filled with water. One can easily observe a marked decrease in the high-frequency content of this record when compared to Fig. 14. We believe that these data indicate that there is a significant viscous transfer of shear wave energy across a rock-water interface. Because the viscous force term increases linearly with frequency, high frequency S_H waves are more efficiently transmitted across a rock-water interface when compared to the transmission of lower frequency S_H waves across an interface. Due to time and equipment limitations, further analysis of this phenomenon has been deferred for the present. If this phenomenon is reproducible (i.e., real), it could provide a useful method of determining whether a crack is filled with a gas or liquid.

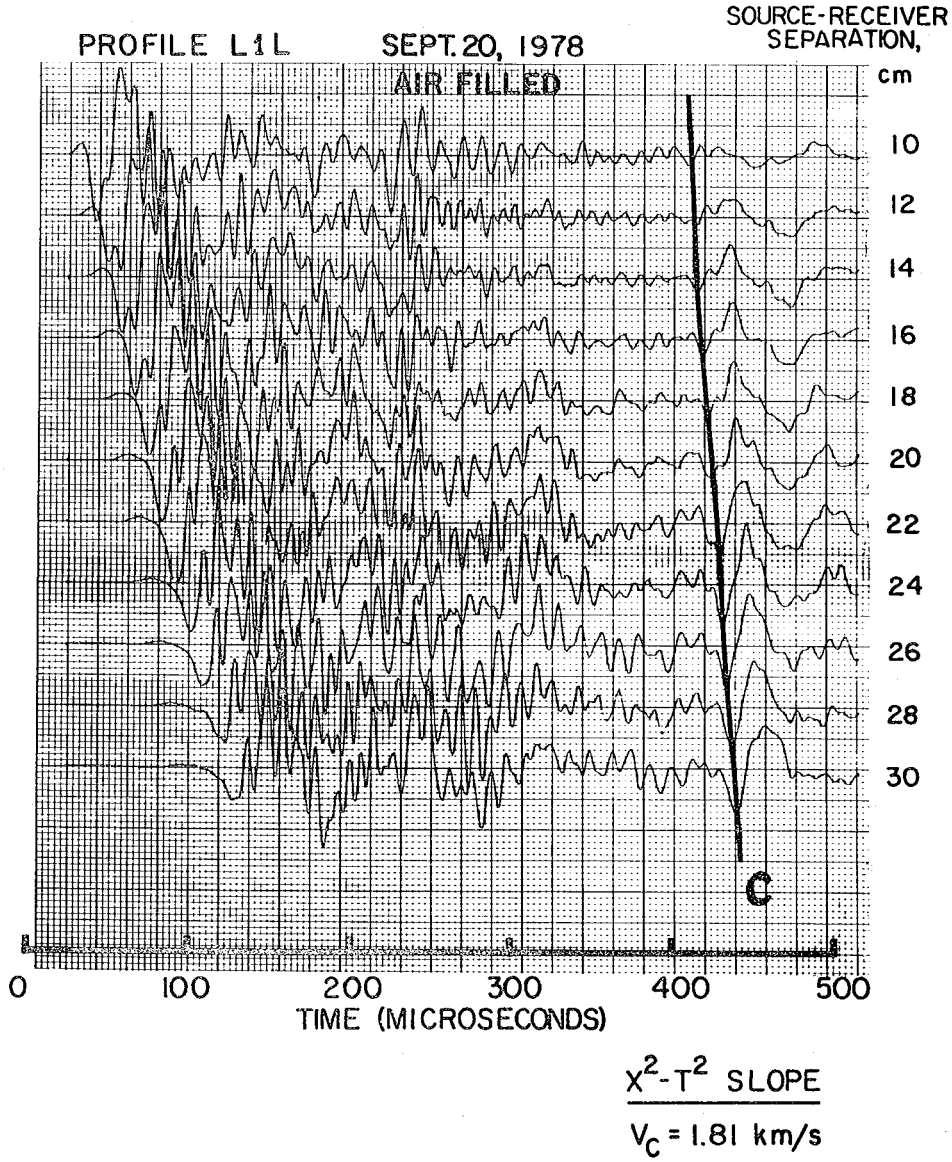

XBL 795-9789

Fig. 14. A profile recorded along line L1L on Sept. 20, 1978. Note the increased "ringiness" of this record when compared to Fig. 13, which presumably indicates further deterioration of the epoxy bond. The crack is air-filled, as is the case in all previous profiles along L1L.

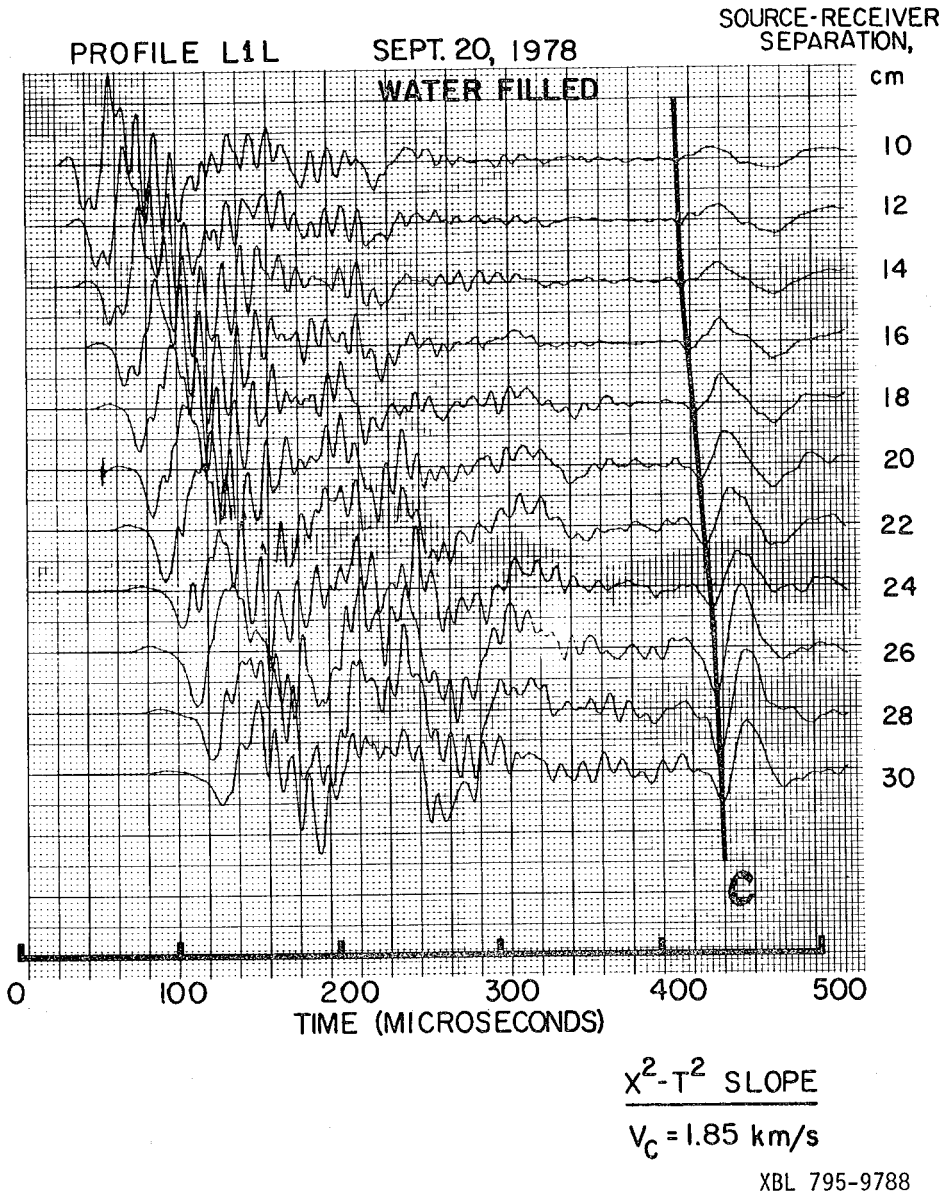

Fig. 15. A profile recorded along line L1L on Sept. 20, 1978, as in Fig. 14, but in this case the crack and axial hole have been filled with water. Note the strong attenuation of the high-frequency energy in this record when compared to Fig. 14, which might be due to viscous coupling of the shear wave into the water.

6. EXPERIMENTS ON METHODS OF REDUCING SURFACE WAVE NOISE

Surface waves, such as direct P and S, Love, and Rayleigh waves, present a source of undesired noise in seismic reflection profiling. Since such surface waves can be thought of as a spatially coherent noise source, temporal averaging of a single seismic trace will not enhance reflection events with respect to the surface wave noise. We have investigated two methods of reducing the surface wave noise:

- Physical scattering of the surface wave
- Use of a directive receiver array

A very simple way of decreasing surface wave noise in a seismic reflection survey is to interpose a surface wave scatterer, such as a slit trench, between the source and receiver. Two such slits, used as lifting holds, are present on the circular face of the cylindrical model (see Fig. 9). A source was located behind one of these slits, so that data taken along L3I would give an indication of the usefulness of this technqiue. The source was placed far enough behind the slit so that the downgoing waves associated with the reflection event would not be severely diffracted by the slit. Figure 16 presents results of a typical multi-trace profile obtained along L3I which can easily be compared to similar multi-trace profiles, such as those recorded along L1L. For small source-receiver separations (12 cm to 16 cm) along L3I, the reflection event is greatly enhanced by the scattering of the surface wave when compared to data obtained with no surface scatterer present (e.g., source-receiver separations of 12 to 16 cm along L1L). From this comparison, it appears that the presence of the slit decreases the amplitude of the surface wave approximately fourfold times with respect to the reflected event. This

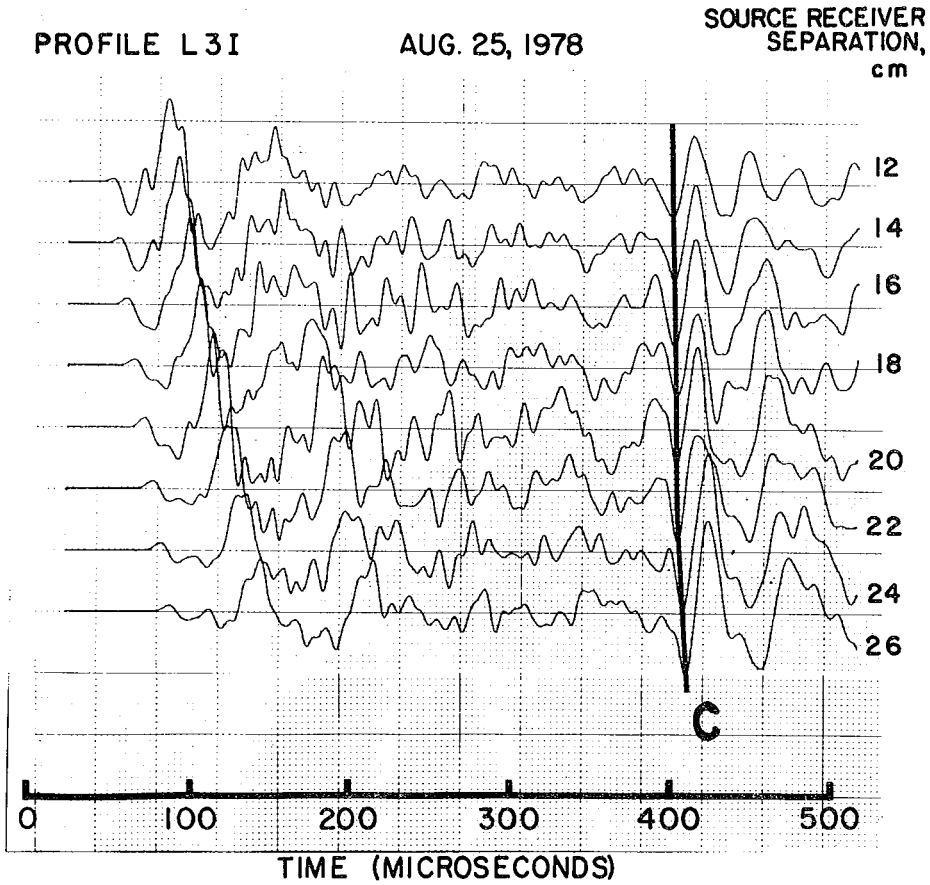

XBL 795-9787

Fig. 16. A multi-trace profile recorded along L3I on Aug. 25, 1978 where the source and receiver are separated by a slit trench (lifting hold) as is shown in Fig. 9. Note the enhancement of the reflected event for source-receiver separations of 12 cm to 16 cm. The velocity information obtained from the slope of the direct event moveout is lost using this technique.

is indeed a significant improvement, but this technique destroys the velocity information contained in the direct P and S_H events.

The use of linear geophone arrays to reduce surface wave noise is a standard practice in petroleum exploration seismology. Various patterns of

detectors can be used to give directivity (direction sensitivity) to the reception of incoming seismic waves. The theory and design of directive receiver arrays is thoroughly reviewed in Waters (1978). A large (2" x 2" x 1/8") S_H sensitive, piezoelectric plate was used as a continuous linear array in this study. This array has to be designed to exhibit good rejection of surface traveling waves in our model experiment.

Figure 17 presents a standard profile recorded along L1R on August 2, 1978, using a small (1/4" x 1/4" x 1/16") point S_H receiver. This receiver should not exhibit any surface wave cancellation because of its small spatial coverage. We have used the trace recorded for a source-receiver separation of 20 cm on L1R for comparison with traces recorded at this location using the linear receiver array. Figure 18 shows a trace recorded along L1R on August 3, 1978 with the center of the receiver array separated 20 cm from the source.

By comparing the amplitude of the reflected event to the amplitude of the initial surface wave event, a measure of the directive properties can be obtained. We believe comparison of Figs. 17 and 18 in this manner shows that the linear array enhances the reflection event by a factor of two when compared to the response of the point S_H receiver. We believe that the large-amplitude event occurring between 170 μs and 250 μs on the trace shown in Fig. 18 is due to a surface traveling P or Rayleigh wave reflected from the axial hole drilled at the center of the circular face. This event would arrive along the linear array in phase and with a particle motion essentially parallel to the S_H polarization. Because of the in-phase arrival, this event is also enhanced with respect to the direct surface waves. From these initial

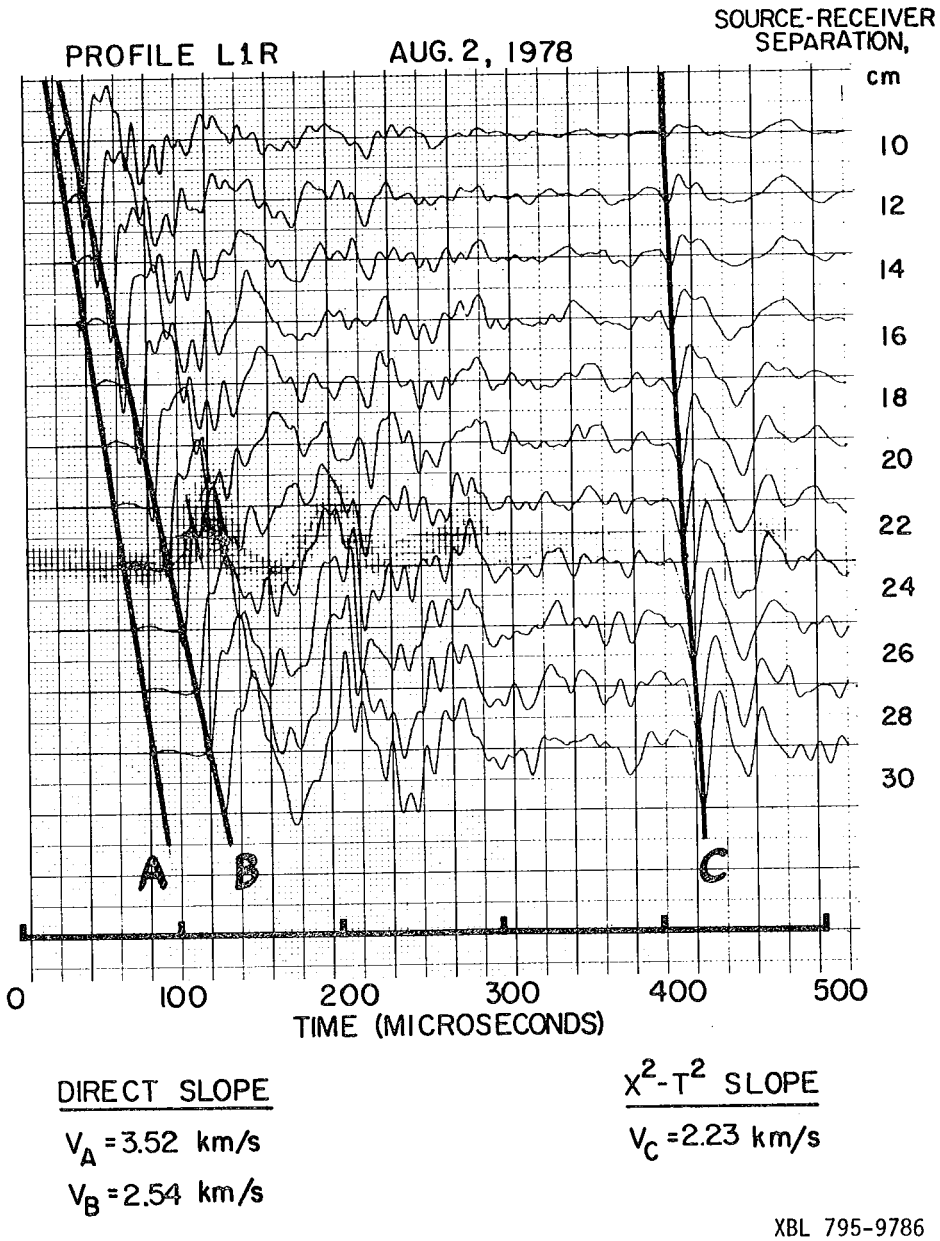

XBL 795-9786

Fig. 17. Profile recorded along L1R on Aug. 2, 1978 with a point S_H receiver. The trace recorded at a source-receiver separation of 20 cm is compared to a trace recorded with a linear receiver array with its geometrical center located 20 cm from the source. For a point receiver, the direct S_H event has about twice the amplitude of the reflected S_H event.

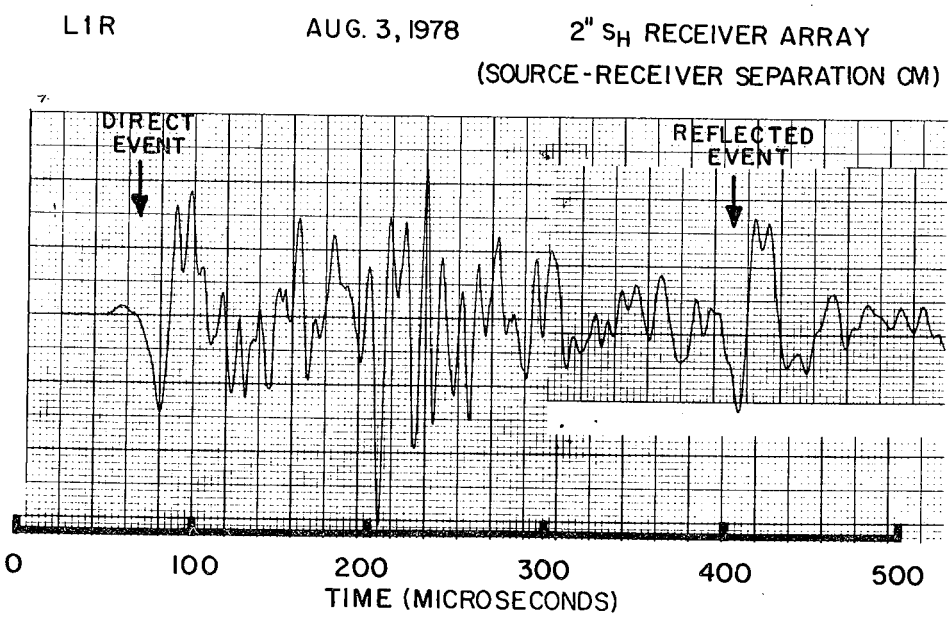

XBL 795-9785

Fig. 18. A seismic trace recorded along line L1R on Aug. 3, 1978 using a 2" S_H linear receiver array. The geometrical center of the receiver array is located 20 cm from the source. The direct and reflected S_H events are of nearly equal amplitude in this figure. Comparison to Fig. 17 indicates that the reflected event amplitude is nearly doubled with respect to the direct event when a receiver array is used to obtain the seismic signal. The large event occuring at ~200 μs is believed to be a surface-travelling P or Rayleigh wave that has been reflected from the axial hole located at the center of the circular face.

experimental results, we believe that these techniques would be worth developing in greater detail.

7. DECONVOLUTION PROCESSING

The character of the waveform emitted from the piezoelectric source strongly influences the appearance of the received waveform. We believe that the records presented in Figs. 13 and 14 show the effect of a changing source

waveform on the received records. Deconvolution processing (undoing the effects of a previous convolution, or filter) is a procedure that replaces each "event" on the seismogram by a symmetrical (zero-phase), band-limited pulse. Deconvolution is simply the convolution of the inverse of the source waveform with the receiver signal. To mathematically describe the deconvolution process, we assume that the received signal $s(t)$ is constructed by summing a series of pulses with varying amplitudes and delay times. Each pulse, designated $f(t)$, represents the functional description of the source wavelet. Thus:

$$s(t) = a_1 f(t-\tau_1) + a_2 f(t-\tau_2) + \ldots + a_n f(t-\tau_n),$$

or

$$s(t) = a_1 \delta(r_1) \otimes f(t) + a_2 \delta(r_2) \otimes f(t) + \ldots + a_n \delta(r_n) \otimes f(t)$$

where $\otimes$ is the convolution operator. The purpose of the deconvolution process is to remove the effect of the source wavelet $f(t)$. This can be done by convolving $s(t)$ with the inverse of $f(t)$, i.e., $f^{-1}(t)$. If an infinite bandwidth is available, the convolution $f(t) \otimes f^{-1}(t)$ will result in $f(t) \otimes f^{-1}(t) = \delta(0)$. However, if the bandwidth of $f(t)$ is limited to interval (ω_1,ω_2), then the result of $f(t) \otimes f^{-1}(t)$ will be a band-limited auto-correlation function $A(\omega_1,\omega_2,t)$. Finally,

$$s(t) \otimes f^{-1}(t) = a_1 A(\omega_1,\omega_2,t) + a_2 A(\omega_1,\omega_2,t) + \ldots + a_n A(\omega_1,\omega_2,t) .$$

In model experiments using the rectangular granite slab, it is possible to estimate the source wavelet $f(t)$ by locating the receiver vertically below the source on the far side of the slab. Figure 19 shows the waveform recorded

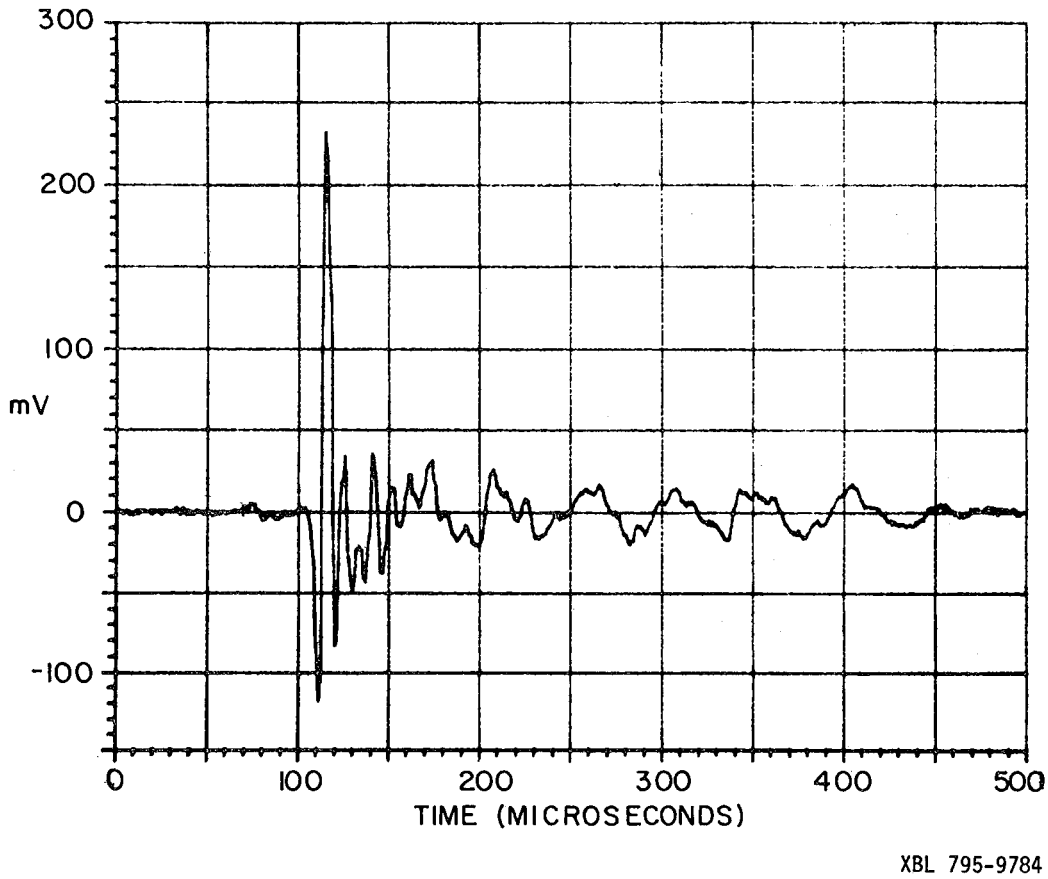

Fig. 19. Waveform recorded directly beneath source on the far face of the rectangular granite slab. This waveform is used as an estimate of source wavelet f(t) in the deconvolution processing.

by a receiver located directly below the source on the far face, so that this waveform may be used to represent the source wavelet f(t). This estimate of f(t) may then be applied to receiver traces s(t) recorded on the top surface of the slab, such as the trace shown in Fig. 20.

We note that the convolution $s(t) \otimes f^{-1}(t)$ can be rewritten as the quotient $\tilde{S}(\omega)/\tilde{F}(\omega)$, where $\tilde{S}(\omega)$ and $\tilde{F}(\omega)$ are the Fourier transforms of s(t) and f(t), respectively. The inverse Fourier transform is then applied to this

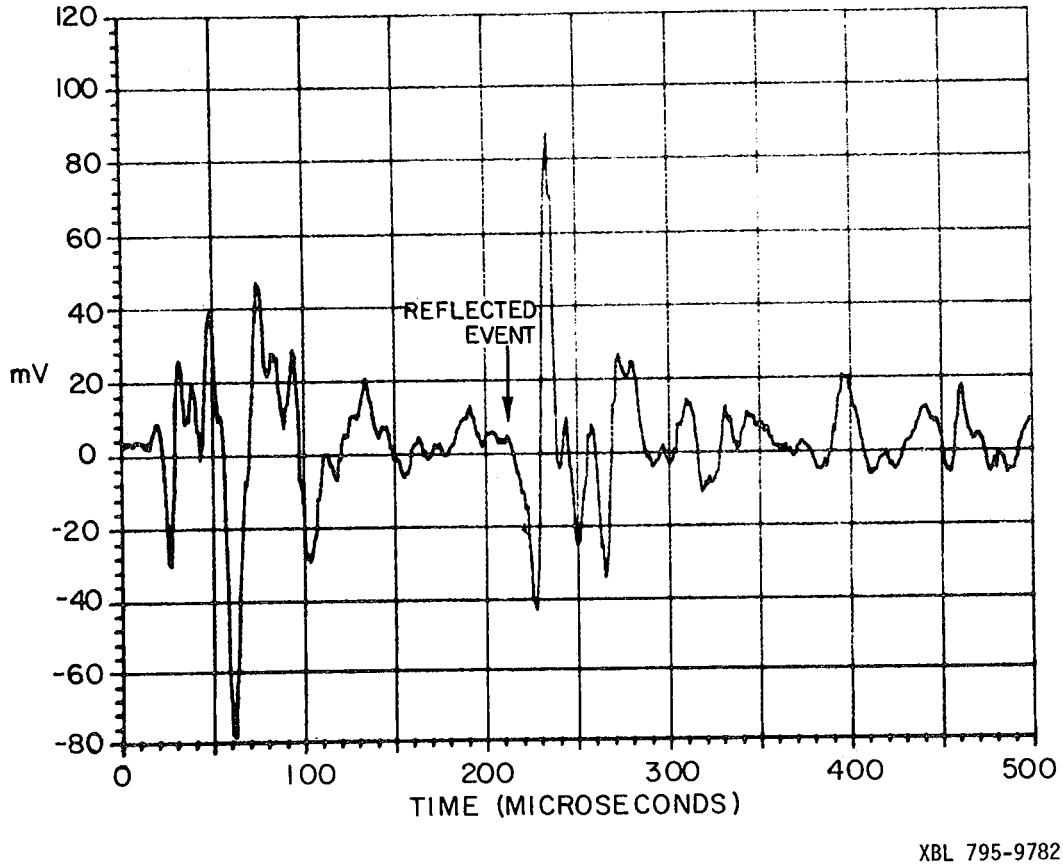

Fig. 20. Waveform recorded on the top surface of the granite slab with a source-receiver separation of 14 cm. This waveform is used to represent the received signal s(t) in the deconvolution processing.

---

quotient to yield the time domain representation of the deconvolved trace, i.e., $s(t) \otimes f^{-1}(t)$. The method used to obtain the deconvolved trace shown in Fig. 21 is outlined as follows:

1. Obtain the Fourier spectrum $\tilde{S}(\omega)$ of the received signal s(t) shown in Fig. 20.
2. Obtain an estimate of the source wavelet f(t). In this case we use the received waveform shown in Fig. 19 as the source wavelet f(t).

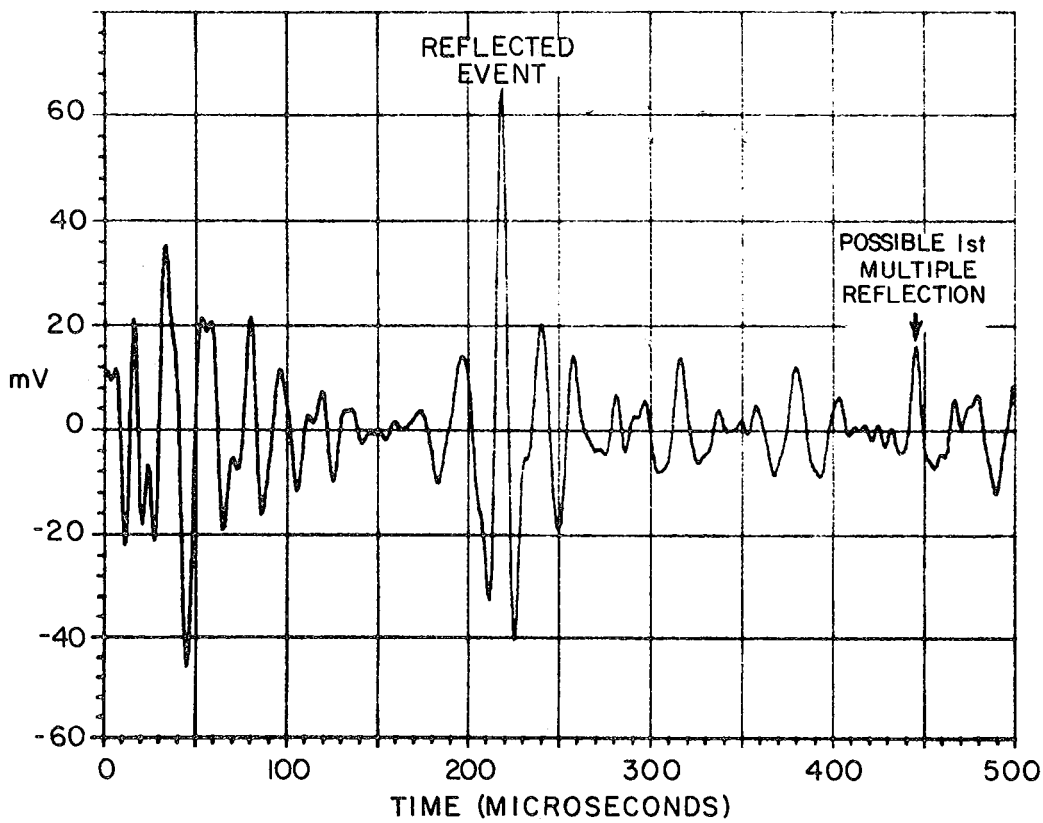

XBL 795-9783

Fig. 21. Deconvolved version of the received signal s(t) shown in Fig. 20. The "ringing" visible in this deconvolved record is due to the boxcar window used in the editing of the quotient $\tilde{S}(\omega)/\tilde{F}(\omega)$.

3. Add a small amount of random noise to f(t). This prevents the problem of dividing by zero when forming the complex quotient $\tilde{S}(\omega)/\tilde{F}(\omega)$.

4. Perform the complex division $\tilde{S}(\omega)/\tilde{F}(\omega)$.

5. Edit the quotient $\tilde{S}(\omega)/\tilde{F}(\omega)$ to limit the spectrum to the frequency limits that exist in the source-generated wavelet. This process

is rather subjective, but can be accomplished using more sophisticated methods than could be implemented within the time limits placed upon us. The editing used in this case was simply a boxcar window spanning the frequencies from ω_1 to ω_2. It is evident in the deconvolved trace of Fig. 21 that this sharp truncation resulted in some"ringing" in the final deconvolved record.

6. Apply the inverse Fourier transform to the quotient $\widetilde{S}(\omega)/\widetilde{F}(\omega)$ to obtain the deconvolved, time-domain record shown in Fig. 21.

The peaked spike occurring around 220 μs in the deconvolved trace of Fig. 21 corresponds to the reflection event of Fig. 20. We believe that the smaller amplitude spike occurring near 445 μs on Fig. 21 represents the first multiple reflection event (path P_4 of Fig. 4). As was previously mentioned, a less "ringy" deconvolved trace could be attained by applying a smoother truncation window to the spectral quotient $\widetilde{S}(\omega)/\widetilde{F}(\omega)$. Because many surface waves (e.g., Love waves) are an interference phenomenon, the spectral content of these surface waves usually will not resemble the spectral character of the source wavelet. Since the reflection coefficient of a rock-fluid interface is possibly frequency independent, then a reflected S_H event will have the same basic spectral characteristics as the source wavelet (ignoring anelastic attenuation). Thus, in certain instances it appears that deconvolution processing will provide another technique useful in reducing surface wave noise. This effect, in addition to the improved arrival time and amplitude data available from the deconvolved record, makes deconvolution processing a very promising technique.

8. CONCLUSIONS AND RECOMMENDATIONS

The purpose of our research is to develop a seismic reflection profiling system that can detect fluid-filled cracks within a crystalline rock mass. Our initial efforts were aimed at developing a working, laboratory-scale reflection profiling system that could be easily modified for larger-scale field studies. Our S_H reflection profiling system has successfully detected an irregular crack (either air- or water-filled) induced with a large laboratory specimen. Experiments simulating a crack closure under an applied stress suggest that it is possible to cause a change in the crack reflection coefficient by varying the normal stress across the crack. Other experiments seem to indicate that the reflection coefficient of the crack depends strongly on the type of fluid filling the crack. This phenomenon may be due to viscous coupling between the rock and fluid media. If this is the case, it may be possible to determine the type of fluid filling the crack through spectral analysis of the reflected waveform.

Model studies performed by Evans (1959) using S_H reflection techniques demonstrate that large amplitude Love waves occur when a thin, low-velocity surface layer is present. Because surface waves represent a source of undesirable noise in seismic reflection surveys, two methods of reducing surface wave noise have been investigated. The first method requires the placement of a scattering body, such as a slit trench, between source and receiver. Surface waves traveling from source to receiver are diffracted by the slit, which causes a consequent decrease in the surface wave amplitude at the receiver. The experimental results of this technique are encouraging; however, some important velocity information is lost through the employment

of this technique. The second method of surface wave cancellation involves the use of linear receiver arrays, a practice that is commonly used in land-based exploration seismology. Our initial experiments suggest that this technique can be successfully applied to high-frequency seismic reflection studies. Other experiments suggest that deconvolution processing (convolution of the inverse of the source input with the received output) can be useful under certain conditions in the cancellation of surface wave noise.

The success of the laboratory-scale S_H reflection profiling system suggests that this system should be modified for larger scale field testing. The ubiquitous presence of a low velocity surface layer in any field situation leads to the emanation of large-amplitude Love waves from an S_H seismic source. The detection of reflected events hidden within this surface wave noise will be an important consideration during field testing of the S_H reflection profiling system. Thus, linear array and deconvolution processing should be performed on the data collected during the field test. Another very important consideration in the future field application of this system will involve the design of a suitable source transducer. The principal difficulty will be in producing a portable, reusable S_H source transducer that is easily bonded to the vertical walls and ceiling of an underground opening.

The data obtained during the laboratory phase of the research will enable a rough estimate of the behavior of the prototype field system. The maximum depth of penetration of the field system will be approximately 10 meters in a reasonably unfractured rock mass. This maximum penetration depth will be significantly less in a highly fractured setting, but no laboratory work has been performed in order to quantify this effect.

In Section 1 it was noted that all incident S_H energy is totally reflected from a crack filled with a non-viscous fluid. This implies that the S_H reflection technique will detect only the nearest fracture beneath the source-receiver pair. This indeed is the case if the nearest fracture is gas-filled, as gases exhibit negligible viscosity. However, water possesses a significant viscosity which must be taken into account when developing the analytical expression for the reflection coefficient of a crack filled with water. The final form of this reflection coefficient will depend on the frequency of S_H wave excitation, the shear wave velocity of the surrounding elastic medium, the viscosity of water (which is temperature-dependent), and the thickness of the crack. At the frequencies used by the S_H field reflection system, theory indicates that incident S_H energy will be totally reflected by water-filled cracks with thicknesses greater than 1.0 mm, and totally transmitted for cracks with thicknesses less than 0.01 mm. Partial reflection will occur for water-filled cracks with thicknesses lying within these bounds. Thus, the maximum depth of penetration of the field system and its resolution of crack thicknesses are interrelated, and both of these quantities depend on the size, structure, and fluid content of the fracture system at that particular field site. Further laboratory and field experimentation will be necessary in order to more exactly quantify these effects.

9. ACKNOWLEDGMENTS

We wish to thank Professors L. R. Johnson and T. V. McEvilly of the Department of Geology and Geophysics, U.C. Berkeley, for their useful advice

and the loan of some excellent ultrasonic transducers, and Dr. P. H. Nelson of the Lawrence Berkeley Laboratory for his generous support. Also, we wish to thank the students and technical staff of the Engineering Geoscience Group, U.C. Berkeley, for their support, and most especially Joe Lamb for his invaluable assistance. Special thanks are due to Prof. H. F. Morrison of the Engineering Geoscience Group, U.C. Berkeley, for his suggestions regarding this research.

10. BIBLIOGRAPHY

Born,M., and Wolf,E. 1975. Principles of optics. Elmsford, N.Y.: Pergamon Press, Inc.

Dampney,C.N.G., Mohanty,B.B., and West,G.F. 1972. A calibrated model seismic system. Geophysics 37 (3): 445-455.

Dobrin,M.B. 1960. Introduction to geophysical prospecting. New York, N.Y.: McGraw-Hill Book Co.

Evans,J.F. 1959. Seismic model experiments with shear waves. Geophysics 24 (1): 40-48.

Gupta,R.R. 1972. Seismic determination of geological discontinuities ahead of rapid excavation. Advanced Research Projects Agency Report No. 6311, 82 pp.

Mason,W.A. 1964. Physical acoustics. In Principles and Methods, Vol. 1 - Part A. Washington,D.C.: Academic Press, Inc.

Price,T.O. 1975. Demonstration of acoustical underground survey system in the Washington metropolitan area. Federal Highway Administration Report No. FHWA-RD-75-82, 106 pp.

Telford,W.M., Geldart,L.P., Sheriff,R.E., and Keys,D.A. 1976. Applied geophysics. New York, N.Y.: Cambridge University Press.

Waters,K.H. 1978. Reflection seismology, a tool for energy resource exploration. New York, N.Y.: John Wiley & Sons, Inc.

Witherspoon,P.A., Amick,C.A., and Gale,J.E. 1977. Stress-flow behavior of a fault zone with fluid injection and withdrawal. Annual Report for period June 1, 1974 to December 30, 1976, to U.S. Geological Survey under contract no. 14-08-0001-14583, 159 pp.

Yu, Thiann-Ruey. 1967. Ultrasonic system for fracture detection in rock faces. M.A. Thesis, McGill University.

Yu,T.R., and Telford,W.M. 1973. An ultrasonic system for fracture detection in rock faces. Canadian Mining and Metallurgical Bulletin 66 (1): 96-101.

This report is part of a cooperative Swedish-American project supported by the U.S. Department of Energy and/or the Swedish Nuclear Fuel Supply Company. Any conclusions or opinions expressed in this report represent solely those of the author(s) and not necessarily those of The Regents of the University of California, the Lawrence Berkeley Laboratory, the Department of Energy, or the Swedish Nuclear Fuel Supply Company.

Reference to a company or product name does not imply approval or recommendation of the product by the University of California or the U.S. Department of Energy to the exclusion of others that may be suitable.